

Martin Rypestøl

Analysis of Floating Offshore Wind Turbine Subjected to Ship Collisions

Master's thesis in Marine Technology

Supervisor: Jørgen Amdahl and Zhaolong Yu

June 2020

NTNU
Norwegian University of Science and Technology
Faculty of Engineering
Department of Marine Technology

Martin Rypestøl

Analysis of Floating Offshore Wind Turbine Subjected to Ship Collisions

Master's thesis in Marine Technology
Supervisor: Jørgen Amdahl and Zhaolong Yu
June 2020

Norwegian University of Science and Technology
Faculty of Engineering
Department of Marine Technology





MASTER THESIS 2020

for

Stud. **Martin Rypestøl**

Analysis of ship / floating offshore wind turbine collisions

Analyse av kollisjon mellom skip og flytende offshore vindturbiner



Background;

In order to develop offshore wind energy beyond low and medium depth coastal areas, several European countries including France are planning to install floating wind farms in the coming years. In the North Sea, 25 km from the Scottish coast of Peterhead, the HYWIND experimental park managed by Statoil is already operational. Wind farms are generally located near the coast, where sea traffic is important. This is the case of the future wind park of Dunkirk in the North Sea or that of Guérande close to the estuary of the river Loire in France. From the safety point of view, the probability of collision of a ship during an avoidance maneuver of another vessel or free drift following a propulsion damage is not negligible. On the other hand, numerical simulations of ship collisions against fixed wind turbine supports such as jacket (Le Sourné, 2015), Amdahl (2013) or monopile (Bela, 2017) and floating (Echeverry, 2019) have clearly shown that for some perfectly realistic scenarios, a relatively low velocity impact can lead to the collapse of the tower support and fall of the nacelle on the deck of the ship. The consequences can be significant: loss of life, perforation of the vessels of the ship causing pollution or explosion in the case of a LNG tanker, damage to impacted wind turbines, rupture of the anchor lines leading to the drift of the platform and to a collision of it against other wind turbines in the park. Finite element analysis can be used to rigorously analyze the resistance of an offshore structure impacted by a ship - Amdahl (2001, 2011), Biehl (2005), Vredevelde (2013), Le Sourné (2015), Bela (2017), Echeverry (2019). Nevertheless, due to the strongly nonlinear behavior of the impacted structures, the geometries of the ship and the wind turbine must be meshed very finely in order to capture the deformation modes (crushing of the structures in contact, plastic bending and buckling of the mast, etc..

Numerical models therefore remain very time consuming, both with respect to model preparation and in computation time (several hours for a collision scenario) and their

development often requires a strong expertise. This is why simplified but fast "super-element" approaches, based on analytical formulations (Le Sourne, 2002, 2012) (Buldgen, 2012a, 2012b, 2014), are of interest to the various actors in the field such as classification organizations and the regulatory authorities for maritime traffic. Risk analyzes, often carried out at the pre-project stage, can include several tens or even hundreds of collision scenarios, given the different types of ships brought to navigate near the parks (DNV, 2013)., Only a few cases can therefore be analysed by nonlinear finite element methods (NLFEM). The project aims to develop and validate a reliable, fast and easy-to-access simulation tool for analyzing ship collisions against floating wind turbines.,

The overall objective is to couple a "mechanical" solver by super-elements to simulate the damage of the structures (ship and wind turbine) during the collision, to a "fluid" solver that simulates the overall movements of the structures during and after the collision. This solver must take into account the hydrodynamic forces that apply to the floats (inertial water masses, hydrostatic restoring forces, dissipative radiation radiation).

Scope of work

The following topics should be addressed:

1. The collision analysis should include a 10 MW turbine in both parked and operating condition. In the operating condition the inertia effects of the rotating blades should be taken into account using a simple constant pitch model. A beam model of the blades shall be established with correct flexibility. The effect of the wind drag and lift forces shall be modelled with equivalent line loads. The model shall be calibrated against the behaviour of an accurate blade model
2. Establish a finite element model for the OO Star Wind Floater including mooring lines. Check that the model is correct wrt. global, rigid body motions. Perform eigenvalue analysis or estimate eigenfrequencies through decay tests. To investigate possible local buckling of the tower at the bottom, this section shall be modelled with shell elements. Local imperfections may need to be established. The local buckling model should be verified against rule formulations.
3. The floater shall be assumed to be fabricated in concrete. Perform analysis of the local damage by establishing a finite element model of a section of the concrete pontoon using LS-DYNA. reference is made to an analysis carried out by Yanyan Sha for the Bjørnefjorden floating bridge. Finite element models of the impacting ship will be made available.
4. Conduct global analysis of the impact with USFOS, where the local indentation of the pontoon and crushing of the ship are modelled with nonlinear springs. Compare the maximum impact forces with punching shear failures strength established in pt.3. Check results with simplified analysis based on the uncoupled approach. Evaluate also crucial response parameters, such as accelerations of tower top and local buckling of tower.
5. Check the outcome of collisions where the ship drift locked to the floater. Are the mooring lines capable of stopping the ship.

6. If this is made possible conduct analysis of glancing blow impacts with representative global motion properties of the ship (waterplane stiffnesses, masses and mass moments of inertia). Compare with simplified uncoupled analysis.
7. Conclusions and recommendations for further work

Literature studies of specific topics relevant to the thesis work may be included.

The work scope may prove to be larger than initially anticipated. Subject to approval from the supervisor, topics may be deleted from the list above or reduced in extent.

In the thesis the candidate shall present his personal contribution to the resolution of problems within the scope of the thesis work.

Theories and conclusions should be based on mathematical derivations and/or logic reasoning identifying the various steps in the deduction.

The candidate should utilize the existing possibilities for obtaining relevant literature.

The thesis should be organized in a rational manner to give a clear exposition of results, assessments, and conclusions. The text should be brief and to the point, with a clear language. Telegraphic language should be avoided.

The thesis shall contain the following elements: A text defining the scope, preface, list of contents, summary, main body of thesis, conclusions with recommendations for further work, list of symbols and acronyms, references and (optional) appendices. All figures, tables and equations shall be numerated.

The supervisor may require that the candidate, in an early stage of the work, presents a written plan for the completion of the work. The plan should include a budget for the use of computer and laboratory resources which will be charged to the department. Overruns shall be reported to the supervisor.

The original contribution of the candidate and material taken from other sources shall be clearly defined. Work from other sources shall be properly referenced using an acknowledged referencing system.

The report shall be submitted in two copies:

- Signed by the candidate
- The text defining the scope included
- In bound volume(s)
- Drawings and/or computer prints which cannot be bound should be organised in a separate folder.

Supervisor:

Prof. Jørgen Amdahl
Postdoc Zhaolong Yu

Deadline: June 10, 2020

Trondheim, January 15, 2020

Jørgen Amdahl

Summary

Floating offshore wind turbines are, like all other offshore structures, exposed to the risk of ship collisions. Future wind farms may be located closer to traffic cargo and passenger lanes, and moving them farther offshore introduces more hostile environments and larger service vessels. The consequences of a ship-FOWT collision can range from minor to major, i.e., from repair cost to injuries or fatalities. This Master's Thesis objective is to study the global and local behavior of the floating offshore wind turbine OO-Star Wind Floater when subjected to ship collision. Finite element analyses have been conducted using LS-DYNA and USFOS.

OO-Star Wind floater is built in post-tensioned concrete, and impacts are considered to follow the strength design principle. In general, this means that the concrete columns are considered as rigid. Two impact-scenarios have been studied: broadside impact and bulbous bow impact by the UT745 Platform Supply Vessel. The force-displacement curves for this ship have been established in LS-DYNA. Additionally, reinforced concrete structures are exposed to punching shear failure due to large localized forces, and a parameter study on different thicknesses have been performed. This study display that for a column thickness of 0.4 m, punching shear can occur. This will lead to flooding of watertight compartments, and endanger the structural integrity of the floating offshore wind turbine.

Global response analyses in USFOS have been performed for both parked and operating turbine. The ship impact is modeled by nonlinear springs containing the force-displacement relationship established in LS-DYNA. The collision energies are based on code formulations, i.e., the impact velocity is 2 m/s for side-impact and 3 m/s for bow impact.

Previous studies have proposed to limit the acceleration of the nacelle to 2-3 m/s, and collision analyses performed in this thesis violates this criterion. The electrical equipment is endangered, which may lead to extensive economic consequences. The turbine tower is an unstiffened cylindrical shell, and local buckling is a risk during a ship impact. In operational condition, impacts normal to the rotor plane are most critical, and buckling is triggered by increasing the speed for sideways impact to 5 m/s. The buckling mode causes the tower to fall in the direction of the ship, posing a real threat to health and safety. The risk of the blades hitting the tower has also been investigated. For the worst scenarios, this event is plausible. However, the modeled tower clearance in USFOS is lower than originally for the 10MW reference wind turbine, so the risk is lower for the real structure. Finally, analyses where the ship and FOWT are locked together after impact has also been investigated. The catenary mooring system is capable of withstanding the forces from this impact scenario.

Generally, accidental loads from ship collisions are critical for the floating offshore wind turbine. Impact analyses in the preliminary design phase are recommended.

Sammendrag

Flytende offshore vindmøller er, i likhet med andre offshore strukturer, utsatt for skipskollisjoner. Fremtidige vindparker kan bli plassert i nærhet av skipstrafikk, og tøffere værforhold sørger også for større forsyningsskip. Ved en kollisjon kan konsekvensene variere. Alt fra mindre reparasjoner til skade av personell er mulig. I denne oppgaven er målet å studere OO-Star Wind Floater når den er utsatt for skipsstøt. Elementanalyse har blitt utført i LS-DYNA og USFOS.

OO-Star Wind Floater er laget i betong, og ved en kollisjon så antas små deformasjoner av søylene. Det vil si at mesteparten av deformasjon skjer i skipet. I denne oppgaven har både skipskollisjon med baug og side blitt analysert. Kraft-deformasjonskurver har blitt beregnet ved å bruke LS-DYNA. Forsterket betong er utsatt for svikt ved store lokale krefter, og dette har blitt analysert. En parameterstudie med ulike tykkelser har vist at slik type svikt er mulig dersom tykkelsen på betongen er mindre enn 0.4 m.

Global respons har blitt analysert i USFOS, og både parkert og operativ turbin har blitt undersøkt. Skipskollisjonen er modellert ved å bruke ulineære fjærer som inneholder kraft-deformasjonskurvene fra LS-DYNA. Relevante standarder for flytende vind turbin strukturer har blitt brukt til å bestemme kollisjonsenergiene for de to ulike scenarioene.

Elektrisk utstyr er utsatt dersom akselerasjonene av toppen blir for store, og tidligere studier har forespeilet at akselerasjonen ikke bør overskride 2-3 m/s. Dette kravet er derimot svært utsatt for å bli overskridet ved en skipskollisjon.

Lokal knekking av turbin tårnet er en risiko ved en skipskollisjon. De mest kritiske tilfellene er når støtet skjer normalt på rotor planet. Knekkning er utløst ved en sideveis hastighet på 5 m/s, og dette scenario fører til at tårnet knekker i retning av skipet. Dette er antatt å være et svært kritisk resultat. For å forhindre kollisjon mellom bladene og tårnet er det som regel stor klaring til tårn. De verste kollisjonsscenarioene fører derimot til en risiko for at dette kan skje. På den andre siden er klaringen som er modellert i USFOS betraktelig lavere en for den faktiske turbinen, så det kan godt hende at den faktiske strukturen er trygg. Helt til slutt er også scenario hvor skipet og flyteren blir låst til hverandre etter kollisjon analysert. Dette gir store krefter i forankringslinene, men systemet klarer å motstå dette.

Generelt sett er skipskollisjon kritisk for den flytende strukturen. Det er derfor anbefalt å utføre kollisjonsanalyser i tidlig design fase, da dette kan påvirke designet.

Preface

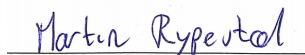
This Master's Thesis is written as a final part of the Master of Science degree, and it is a continuation of the author's Project Thesis. The master was assigned by the Institute of Marine Technology at the Norwegian University of Science and Technology. Professor Jørgen Amdahl has formulated the problem text.

The topic for this thesis is ship collisions with a floating offshore wind turbine. The floating structure chosen for this work is the OO-Star Wind Floater concept developed by Dr. techn. Olav Olsen AS.

The master thesis has provided a greater understanding of the theory and calculation methods regarding ship-FOWT collision and relevant standards and consequences. The majority of the time has been spent on modeling in USFOS and the ship collision analyses. The local analyses in LS-DYNA also proved to be more challenging and time-consuming than initially anticipated.

The work has been challenging and interesting, but particularly motivating considering the limited research on the topic.

Throughout the semester, weekly meetings with my supervisor have provided guidance and motivation for this thesis. Due to the Covid-19 situation, the semester turned out different than expected. The meetings have been completed online, using Microsoft Teams. I would like to thank my supervisor Professor Jørgen Amdahl for all the help. I would also like to thank my co-supervisor Postdoc Zhaolong Yu for help with the LS-DYNA analysis. Finally, I would like to thank Tore Holmås for all the help and guidance with the modeling in USFOS.



Martin Rypestøl
Trondheim, June 7, 2020

Table of Contents

Summary	i
Preface	iii
Nomenclature	xii
Abbreviations	xiii
1 Introduction	1
1.1 Scope of work	3
1.2 Approach	3
2 Background	5
2.1 Floating wind installations	6
3 Design principles	7
3.1 DNV GL and Bureau Veritas	7
3.2 Design values	8
3.3 Energy consideration	8
3.3.1 External and internal mechanics	9
4 Impact scenario and consequences	13
4.1 Consequences	15
5 FEA using LS-DYNA and USFOS	17
5.1 USFOS	17
5.2 LS-DYNA	19
5.2.1 Shell elements	20
6 Finite element models in USFOS	21
6.1 10 MW turbine	21
6.1.1 Tower clearance	24

6.1.2	Model verification	25
6.2	OO-Star Wind Floater	27
6.3	Assembled model	32
6.4	Model verification	32
6.5	Ship collision model	35
7	Local analyses in LS-DYNA	37
7.1	Design ship	37
7.1.1	Shipside model	39
7.1.2	Bow model	40
7.2	Force-displacement curves	40
7.2.1	Shipside	41
7.2.2	Bow	42
7.2.3	Recommended force-displacement relationship	44
7.3	Punching shear	47
8	Global analysis in USFOS	51
8.1	Model verification	52
8.2	Collision analyses for wind turbine in parked condition	54
8.2.1	Moment in tower	54
8.2.2	Acceleration of nacelle	58
8.2.3	Kinetic energy	59
8.2.4	Distance between blade tip and tower	61
8.2.5	Mooringline forces	62
8.3	Collision analyses for wind turbine in operating condition	63
8.3.1	Moment in tower	63
8.3.2	Acceleration of the nacelle	66
8.3.3	Distance between blade tip and tower	68
8.3.4	Mooringline forces	70
8.3.5	Operation in damaged condition	74
9	Discussion and conclusion	77
10	Further work	79
	Bibliography	i
	Appendices	I
A	Punching shear check for concrete column	I
A.1	Ship side 1 m ²	I
A.2	Ship side 6 m ²	III
A.3	Ship bulb 1 m ²	IV
A.4	Ship bulb 6 m ²	VI

List of Figures

1.1	Annual offshore wind installations and cumulative capacity (<i>Key trends and statistics 2019 2020</i>)	1
1.2	Share of substructures for OWT according to <i>Key trends and statistics 2019 (2020)</i>	2
2.1	Offshore wind facilities (<i>Bureau of Ocean Energy Management 2020</i>) . . .	5
2.2	Floating foundations for wind turbines (DNVGL-ST-0119 2018)	6
2.3	OO-Star Wind Floater (Olav Olsen AS 2020)	6
3.1	Ship impact design principles (N-004 2004)	9
3.2	Decoupled problem for ship grounding (Hong 2009)	10
3.3	Load-Deformation relationship N-004 (2004)	11
3.4	Recommended force-displacement relationships (N-004 2004)	11
4.1	Collapse OWT (Biehl and Lehmann 2006)	16
5.1	Livesley functions (Moan 2003)	18
6.1	Three dimensional beam element in USFOS (<i>USFOS USER'S MANUAL-MODELLING 1999</i>)	22
6.2	Blade model in USFOS with structural twist	22
6.3	Velocity and forces on a blade segment (Brøndsted and P.L Nijssen 2013)	23
6.4	Rotational velocity at rotor centre	24
6.5	Tower clearance description according to Bak et al. (2013)	25
6.6	Reference turbine USFOS	26
6.7	Main dimensions OO-Star Wind Floater 10 MW (W. Yu, Müller, and Lemmer 2018)	27
6.8	Coordinate system OO-Star Wind Floater 10 MW (W. Yu, Müller, and Lemmer 2018)	28
6.9	Material density division	29
6.10	Nodal displacement at tower intersection in global z-direction	29

6.11	Mooring system (W. Yu, Müller, and Lemmer 2018)	30
6.12	Mooring system model in USFOS	31
6.13	Pretension in mooring line	31
6.14	Nodal displacement at intersection between turbine tower and OO-Star	33
6.15	CoG and CoB USFOS	34
6.16	Buoyancy force USFOS vs LIFES50+	34
6.17	Collision system for bow in USFOS	35
6.18	Collision system for ship side in USFOS	36
7.1	UT 745 Platform Supply Vessel (<i>Yno 227 - Maersk Frontier</i> 2020)	38
7.2	Columns exposed to ship impact (W. Yu, Müller, and Lemmer 2018)	38
7.3	Shipside model in LS-DYNA	39
7.4	Boundary conditions prescribed node set shipside	39
7.5	Ship bow model in LS-DYNA	40
7.6	Crushing of ship side	41
7.7	Force-displacement curve ship side	41
7.8	Crushing of bulbous bow LS-DYNA	42
7.9	Force-displacement curve forecastle	43
7.10	Force-Displacement curve Bulb	44
7.11	Force-Displacement curves DNV GL (Amdahl, Solland, and Reitan 2017)	45
7.12	Force-displacement curve for supply vessel bow against rigid column	45
7.13	Force-displacement curve for supply vessel bow against rigid column with varying radius (Storheim 2015)	46
7.14	Basic control perimeter around loaded area <i>Eurocode 2</i> (2004)	48
7.15	Nodal points used for force extraction ship side	49
7.16	Punching shear design ship side	49
7.17	Punching shear design ship bulb	50
8.1	Collision scenarios description	52
8.2	Comparison force-displacement curves forecastle and bulb	53
8.3	Linear spring bulb	53
8.4	Comparison force-displacement curves ship side	54
8.5	Equilibrium path for perfect and imperfect shells according to Amdahl (2010)	55
8.6	Acceleration of nacelle side impact parked condition	58
8.7	Acceleration of nacelle bow impact parked condition	59
8.8	Side impact on column 2	60
8.9	Kinetic energy and force displacement curves ship side collision	60
8.10	Relative distance tower and blade tip in parked condition	61
8.11	Layout description for blades in parked condition	61
8.12	Collision scenarios description	63
8.13	Eigenmode shell substructure	65
8.14	Local buckling of tower	66
8.15	Acceleration of nacelle side impact operating condition	67
8.16	Acceleration of nacelle bow impact operating condition	67
8.17	Relative distance between tower and blade tip	68

8.18	Structural behavior during normal operation	69
8.19	Relative distance between tower and blade tip in normal operation	69
8.20	Relative distance between tower and blade tip with impact after 120 seconds.	70
8.21	Force-displacement curve mooring line	71
8.22	Force-displacement curve mooring line	72
8.23	Maximum mooring line force compared to code specifications	73
8.24	Flooded compartments	74
8.25	Waterplane OO-Star Wind Floater	75
A.1	Punching shear ship side, d=0.5	I
A.2	Punching shear ship side, d=0.4	II
A.3	Punching shear ship side, d=0.3	II
A.4	Punching shear ship side, d=0.5	III
A.5	Punching shear ship side, d=0.4	III
A.6	Punching shear ship side, d=0.3	IV
A.7	Punching shear ship bulb, d=0.5	IV
A.8	Punching shear ship bulb, d=0.4	V
A.9	Punching shear ship bulb, d=0.3	V
A.10	Punching shear ship bulb, d=0.5	VI
A.11	Punching shear ship bulb, d=0.4	VI
A.12	Punching shear ship bulb, d=0.3	VII

List of Tables

4.1	Magnitude of consequence of ship collision (Presencia and Mahmood Shafiee 2018)	15
4.2	Potential impacts according to Moulas, M. Shafiee, and Mehmanparast (2017)	15
6.1	Key parameters 10MW Reference Wind Turbine	21
6.2	Regular steel properties	24
6.3	Natural frequencies for the isolated blade	26
6.4	Natural frequencies for the whole turbine	26
6.5	Platform parameters for OO-Star Wind Floater (W. Yu, Müller, and Lemmer 2018)	28
6.6	Material properties OO-Star Wind Floater	29
6.7	Mooring system properties (W. Yu, Müller, and Lemmer 2018)	30
6.8	Added mass and drag coefficients in USFOS	32
6.9	Natural period in pitch for OO-Star Wind Floater	33
6.10	Tower and platform parameters (W. Yu, Müller, and Lemmer 2018)	33
7.1	Main data UT 745 (<i>Yno 227 - Mærsk Frontier</i> 2020)	37
7.2	Force displacement curve for supply vessel side in USFOS	42
7.3	Force displacement points forecastle	43
7.4	Force displacement points bulb	44
7.5	Loading and control perimeter 1 m ²	48
7.6	Loading and control perimeter 6 m ²	48
8.1	Parameters ship impacts in USFOS	51
8.2	Properties lower segment of wind turbine tower	55
8.3	Stresses in tower for ship bow impact in parked condition on Column 1	56
8.4	Stresses in tower for ship side impact in parked condition on Column 1	57
8.5	Stresses in tower for ship bow impact in parked condition on Column 2	57
8.6	Stresses in tower for ship side impact in parked condition on Column 2	57
8.7	Stresses in tower for ship bow impact in operating condition on Column 1	63

8.8	Stresses in tower for ship side impact in operating condition on Column 1	64
8.9	Stresses in tower for ship bow impact in operating condition on Column 2	64
8.10	Stresses in tower for ship side impact in operating condition on Column 2	64
8.11	Breaking load for mooring chain	72
8.12	Proof load for mooring chain	72
8.13	Working load limit for mooring chain	73

Nomenclature

Variable	Unit	Description
a_i	kg	Added mass of installation
a_s	kg	Added mass of approaching vessel
A	m^2	Element area
A_s	m^2	Shell element area
\mathbf{C}	kg/s	Damping Matrix
c	m/s	Acoustic wave speed
C	-	Buckling coefficient
C_D	-	Drag coefficient
C_L	-	Lift coefficient
d	m	Effective depth of concrete column
δ	m	Imperfection tolerance
dw	m	Deformation in force-displacement relationship
ε_x	-	Axial strain
E	Pa	Young's modulus
E_c	J	Colliding vessel energy
E_s	J	Strain energy
$E_{s,i}$	J	Strain energy installation
$E_{s,s}$	J	Strain energy ship
f_{cd}	Pa	Design compressive strength
f_{ck}	Pa	Characteristic compressive strength
F_{imp}	N	Impact force
F_D	N	Drag force
F_L	N	Lift force
g	m/s^2	Gravitational acceleration
k	N/m	Spring stiffness
\mathbf{K}	N/m	Stiffness Matrix
L	m	Element length
λ_e	m	Characteristic length of element
$\bar{\lambda}_{eq}^2$	-	Slenderness parameter
\mathbf{M}	kg	Mass Matrix
M_o	Nm	Overtopping moment
M_u	Nm	Uprighting moment
m_i	kg	Mass of installation
m_s	kg	Mass of approaching vessel
η	-	Utilization factor

P	Pa	Pressure
ρ	kg/m ³	Density
ρ_1	-	Reinforcement ratio
R	N	Force in force-displacement relationship
r	m	Displacement vector
$\dot{\mathbf{r}}$	m/s	Velocity vector
$\ddot{\mathbf{r}}$	m/s ²	Acceleration vector
σ_b	Pa	Bending stress
σ_E	Pa	Elastic buckling strength
$\sigma_{eq,cr}$	Pa	Critical stress
σ_Y	Pa	Yield stress
σ_x	Pa	Axial stress
t	m	Thickness
Δt	s	Length of time step
u_0	m	Length of loading perimeter
u_1	m	Length of control perimeter
v_i	m/s	Speed of installation
v_s	m/s	Speed of approaching vessel
V_0	m/s	Rated wind speed
ν_{Ed}	Pa	Shear stress
V_{Ed}	N	Shear force
$\nu_{Rd,max}$	Pa	Shear stress capacity
W	m/s	Relative velocity
ϕ	-	Shape function Livesley
ω_{max}	Hz	Largest natural frequency
ω	rad/s	Rotational speed
Z_l	-	Curvature parameter

Abbreviations

ALS	Accidental Limit State
CoB	Center of buoyancy
CoG	Center of gravity
CPU	Central Processing Unit
DTU	Danmarks Tekniske Universitet
FEA	Finite Element Analysis
FOWT	Floating Offshore Wind Turbine
GM	Metacentric height
MSL	Mean Surface Level
NFEA	Nonlinear Finite Element Analysis
OWT	Offshore Wind turbine
PSV	Platform Supply Vessel
RWT	Reference Wind Turbine
rpm	rounds per minute
SOV	Service Operation Vessel

Chapter 1

Introduction

Wind energy is a renewable energy source that has been utilized for several years, mainly as onshore installations. Today, the number of offshore installations increases, and the growth will continue in the coming years. Over 500 OWTs was connected to the grid in 2019, giving a cumulative offshore wind capacity of around 22 GW in Europe (*Key trends and statistics 2019 2020*). Figure 1.1 display the annual offshore wind installations and cumulative capacity by country.

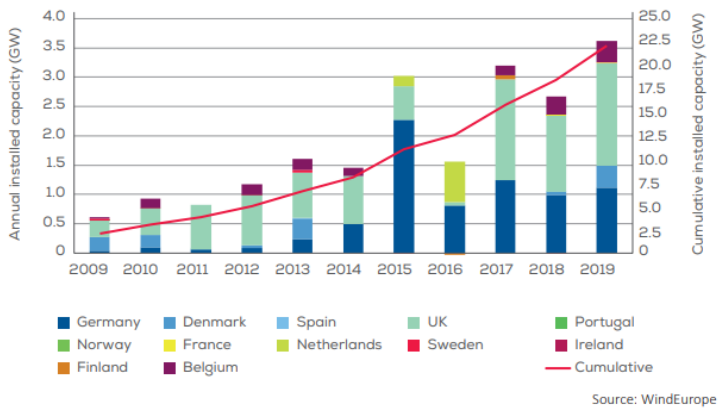
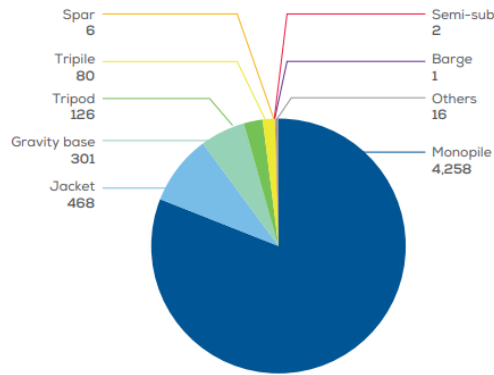


Figure 1.1: Annual offshore wind installations and cumulative capacity (*Key trends and statistics 2019 2020*)

The United Kingdom ranks first with a total offshore wind power capacity of 9.9 GW, followed by Germany with 7.4 GW and Denmark with 1.7 GW capacity. Although the majority of the capacity comes from bottom fixed structures, Europe’s floating fleet is the largest in the world with a total capacity of 45 MW by the end of 2019.

Offshore installations have several benefits compared to onshore wind farms, among these are more stable and steady wind flow and less noise and visual impacts. Higher and more steady wind speeds means that the resource potential is greater offshore than onshore. However, production costs are higher and installations are more advanced.

Offshore wind turbines have in a large extent been limited to bottom-fixed support structures where experience from the oil and gas industry and onshore wind farms have been utilized. 81 % of the installations use monopile foundation, followed by jacket and gravity-based structures.



Source: WindEurope

Figure 1.2: Share of substructures for OWT according to *Key trends and statistics 2019 (2020)*

The wind farms capacity continue to get bigger and bigger and the average rated turbine power was 7.8 MW in 2019. Improvements to wind turbine support structures are important in order to keep up with the rapid development in turbine size.

The full potential of the offshore wind market is unlocked by introducing floating installations. With this technology, deeper water sites can be accessed, and harsher environments can be utilized. However, this makes the installations largely exposed to hazards associated with collisions, either by commercial ships or support vessels (Moulas, M. Shafiee, and Mehmanparast 2017). Numerical simulations of ship collision with bottom fixed foundations have clearly shown that this accidental action can cause collapse of the tower support and a risk for the nacelle to fall onto the ship deck (Echeverry et al. 2019).

1.1 Scope of work

The initial scope of work is defined at the beginning of this report, and it has been discussed with the project supervisor Professor Jørgen Amdahl throughout the semester. The following modifications have been agreed:

Topic 6 - Analysis of glancing blow impacts

This topic is not included. The main reason is that, as of today, USFOS is not prepared for this analysis.

1.2 Approach

The thesis is structured by a general background study on floating offshore wind installations in Chapter 2. This is followed by a chapter describing design principles that apply for ship collision analyses and relevant standards developed for floating offshore wind turbine structures. Chapter 4 describe the most relevant ship collision scenarios and consequences for OWT. Two different finite element programs are used to investigate the structural response by ship impacts: USFOS and LS-DYNA. The main theory and principles behind these programs are described in Chapter 5. The following chapter describes the finite element model in USFOS and how the global analyses are set up, while the local analyses in LS-DYNA are described in Chapter 7. The global results are evaluated in Chapter 8, while discussion and conclusion are presented in Chapter 9. Recommendations for further work are given in Chapter 10.

Chapter 2

Background

Wind energy is a renewable energy source, and wind farms are located both onshore and offshore. New offshore wind farms now operate at up to 55 % capacity, which is a more considerable utilization than onshore installations (*Wind energy today 2020*). Harder and more uniformly distributed winds are some of the main benefits of locating wind farms offshore. However, increased work within design and engineering is necessary to establish offshore facilities. Site-specific conditions, in particular water depth, wave loading, and seabed geology, plays a significant role in determining which facility that is most adequate (*Bureau of Ocean Energy Management 2020*).



Figure 2.1: Offshore wind facilities (*Bureau of Ocean Energy Management 2020*)

Statistics presented in Chapter 1 display that bottom-fixed foundations are the governing support structure of offshore wind turbines. However, moving the wind farms to deeper water depths make floating installations more suitable.

2.1 Floating wind installations

Floating offshore wind turbines (FOWTs) consist of a floating foundation connected to the seabed by mooring lines. Among the floating foundations, the most common types are spar floater, tension leg platform, and semi-submersible foundation (X. Wang et al. 2018).

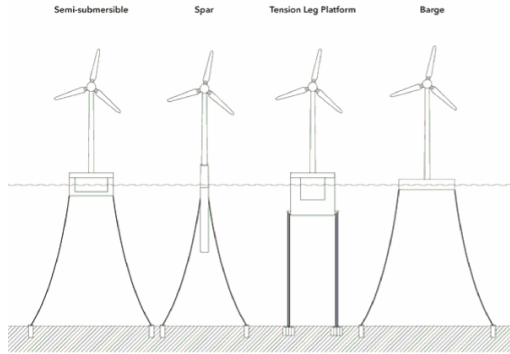


Figure 2.2: Floating foundations for wind turbines (DNVGL-ST-0119 2018)

The barge is a free-surface stabilized structure with a large water-plane area and small draught. The semi-submersible foundation is a buoyancy and free surface stabilized structure, and the spar floater is a weight-buoyancy stabilized structure with large draught. Finally, the TLP foundation is moored vertically and kept in position by tethers or tendons. (DNVGL-ST-0119 2018).

In this thesis, the floating foundation investigated is the OO-Star Wind Floater concept developed by Dr. techn. Olav Olsen AS. The rated power of the wind turbine is 10 MW. Figure 2.3 displays the FOWT, and multiple different ship collision scenarios on this structure are evaluated throughout this thesis.



Figure 2.3: OO-Star Wind Floater (Olav Olsen AS 2020)

Design principles

In this chapter, some of the main features when designing floating wind turbine structures are highlighted, especially considering accidental actions such as ship collisions. DNV GL and Bureau Veritas have both launched standards in recent years specifically for FOWT, while NORSOK N-003 is a standard that applies for bottom fixed and floating offshore structures.

3.1 DNV GL and Bureau Veritas

DNVGL-ST-0119 (ibid.) and Veritas-NI-572 (2019) are dedicated standards for floating offshore wind turbine structures. These two standards similarly classify impact loads. Impacts from approaching boats in normal operation are defined as functional loads, while impacts from drifting boats are defined as accidental loads (DNVGL-ST-0119 2018). In accidental limit state, the characteristic loads shall be taken as the expected loads from the maximum authorized service vessel that can approach the FOWT. Ship added mass effects should be included for all load cases.

For design against accidental boat impacts, DNVGL-ST-0119 (ibid.) specify that the service vessel shall be assumed to drift laterally with a speed of minimum 2.0 m/s. ALS design shall be carried out for the two following situations (ibid.):

- Check the resistance of the structure against design loads
- Check the post-damage resistance against environmental loads. For example, when the impact cause structural damage to the FOWT.

With respect to the consequences of a ship collision, the DNV GL standard specifies that it is governed by the ratio between masses and stiffnesses of the two colliding structures. Damage stability in Veritas-NI-572 (2019) is defined as the FOWT's ability to withstand flooding accidents after a collision, grounding or other accidental conditions. The impact loads may be assessed by different methods:

- Dynamic analysis of vessel approach
 - Should consider vessel displacement and added mass, vessel speed according to sea state and deformation properties.
- Prescriptive method
 - Impact force may be taken as: $F_{imp} = \sqrt{2kE_c}$ where k is the total spring stiffness of the structure at the impact point and E_c is the colliding vessel energy.
- If no data is available the impact force is given by $2.5m_s$, where m_s denote the displacement of the approaching vessel.

The energy of the striking vessel E_c is calculated as:

$$E_c = \frac{1}{2}(m_s + a_s)v_s^2 \quad (3.1)$$

3.2 Design values

NORSOK N-003 is a standard that applies for all types of offshore structures, both floating and bottom fixed. The main focus for this standard is structures involved in petroleum activity. However, it specifies design values that should be used in a risk assessment if no operational restrictions are implemented (N-003 2017).

- Displacement of supply vessel not less than 10 000 tons.
- Head-on collision velocity should be set to 3,0 m/s.
- For sideways and stern impacts, the velocity is set to 2,0 m/s.
- Added mass of ship: 40 % for side impact and 10 % for bow impact.

3.3 Energy consideration

Ship collision loads are characterized by kinetic energy. The energy is described by the mass, hydrodynamic added mass, and the speed of the ship and floating installation when the collision occur (N-004 2004). In the event of a collision, parts of the available kinetic energy can remain as kinetic after the impact, while the remainder is dissipated as strain energy. Structural deformations store the strain energy in the installation and, possibly, in the vessel. The impact conditions are governing for the energy distribution, and large plastic strains and structural damage are in general involved in this energy dissipation.

NORSOK distinguishes between three different design principles for energy dissipation based on relative energy absorption capabilities. As indicated in Figure 3.1, the distribution depends on the relative strength of the two structures (Moan 2003).

- **Strength design**

The installation is strong and will resist the collision force with minimal deformations. Hence, the majority of energy is dissipated by the ship.

- **Ductility design**

The installation dissipates the majority of the energy, causing large plastic deformations.

- **Shared-energy design**

The ship and the installation both contribute to the energy dissipation

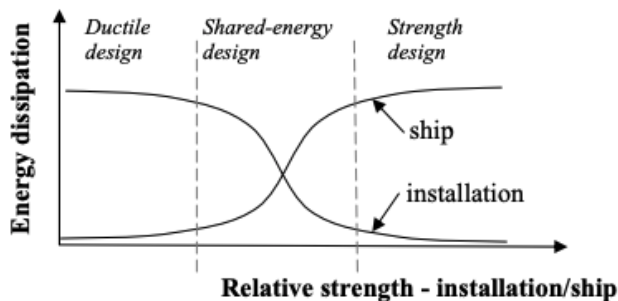


Figure 3.1: Ship impact design principles (N-004 2004)

For calculation purposes, one of the two extremes is favorable, i.e., either ductile or strength design. For these cases, the response of the softest structure can be simplified based on considerations for the "rigid" structure (N-004 2004). Simple calculation methods can then be applied. The complexity of the problem increases in the shared-energy design. In this case, the structural deformation of both structures influences the magnitude and distribution of collision forces. In order to accurately estimate the response, nonlinear finite element analysis must be applied.

3.3.1 External and internal mechanics

A convenient method to deal with the complexity of the fluid-structure problem is to decouple the problem into external dynamics and internal mechanics. The first model assumes constant added mass so that the system is undamped. Hence, the conservation of momentum can be applied, which allows for fast estimations of dissipated energy (Z. Yu et al. 2016). Considering that the velocity of both involved structures are known before and after an impact, the energy loss during the collision can be calculated by external dynamic models.

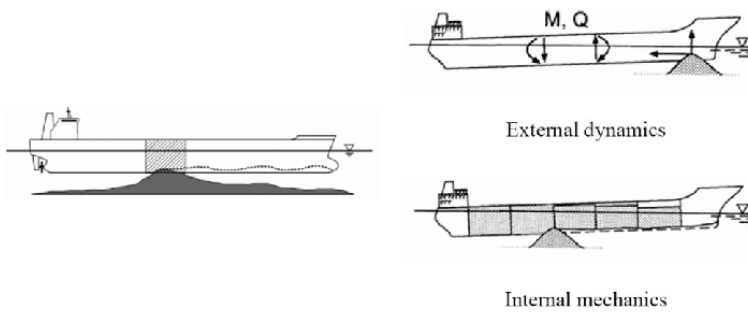


Figure 3.2: Decoupled problem for ship grounding (Hong 2009)

Dissipated energy

To determine the amount of kinetic energy that is dissipated as strain energy, conservation of momentum and energy are applied. Floating structures are according to NORSOK N-004 (2004) considered as compliant installations and the strain energy is given by:

$$E_s = \frac{1}{2} (m_s + a_s) v_s^2 \frac{\left(1 - \frac{v_i}{v_s}\right)^2}{1 + \frac{m_s + a_s}{m_i + a_i}} \quad (3.2)$$

E_s - Strain energy

m_s - Ship mass

m_i - Mass installation

a_s - Ship added mass

a_i - Installation added mass

v_s - Impact speed

v_i - Velocity of installation

In many cases, it is assumed that the installation has zero velocity, which yields $v_i=0$. The collision energy is therefore determined based on properties of the ship:

$$E_c = \frac{1}{2} (m_s + a_s) v_s^2 \quad (3.3)$$

Conservation of energy and momentum are then applied to calculate the amount of energy that remains kinetic after the impact, and what velocity the objects has at the end of impact.

Load-Deformation Relationship

In the assessment of internal mechanics, the strain energy is dissipated by structural deformations. In Figure 3.3 the relationship between the force, R , and the deformation, dw , for the two colliding structures is illustrated.

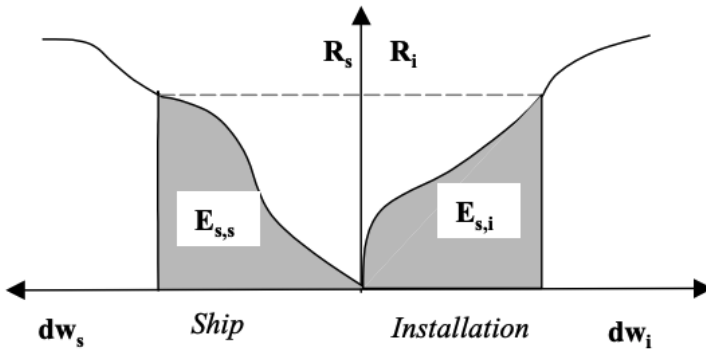


Figure 3.3: Load-Deformation relationship N-004 (2004)

The total area under the curves equals the total strain energy that is dissipated by the structures. The final penetration is considered when the area under the force-displacement curve equals the energy loss during the collision:

$$E_s = E_{s,s} + E_{s,i} = \int_0^{w_{s,max}} R_s dw_s + \int_0^{w_{i,max}} R_i dw_i \quad (3.4)$$

The load level is in general not known in advance, so incremental procedures are often applied to estimate the deformations. It is normal to establish the load-displacement curves for the two structures independently of each other. This is possible by assuming the other structure as being infinitely rigid. In reality, this is a method with limitations as both structures will dissipate energy irrespective of relative strength (Moan 2003). Another issue regarding this is that the response of the more robust structure often is overestimated. The latter is because as the softer structure deforms, the contact area will increase, which will lead to larger resistance of the more robust structure.

Recommended curves for a 5000 tons supply vessel are given in NORSOK N-004 (2004). Figure 3.4 display curves for broad side, stern corner, stern end and bow impact against an infinitely rigid cylinder with varying diameter.

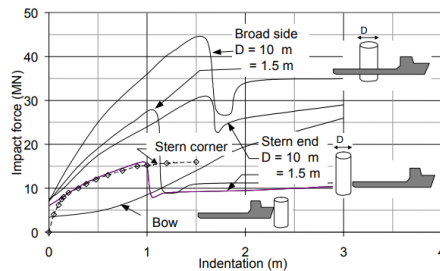


Figure 3.4: Recommended force-displacement relationships (N-004 2004)

The rigid cylinder implies that the curves are based on strength design. If this condition is not met the code specify that interaction between the structures shall be considered. Employing nonlinear finite element methods or simplified plastic techniques are then necessary.

The theory described in this chapter is general with respect to ship impacts, and it will be referenced to throughout the report. However, some results from the analyses requires additional theory, and this is taken into consideration later on. From the analyses, punching shear failure and local buckling are investigated, and the theory behind these checks is presented in the same section as the results. The main reason behind this choice is to get a better understanding of the parameters used in the calculations.

Impact scenario and consequences

Offshore wind farms are growing in size, and with the development of floating installations, addressing deeper water sites is possible. Locating the farms closer to traffic cargo and passenger lanes increase the risk for ship collision (Echeverry et al. 2019). Additionally, moving the farms farther offshore introduces a more hostile environment and larger service vessels. The probability of collision between service vessels and offshore wind turbines, therefore, increases (Dai et al. 2013).

Collision between ship and offshore structures is of great concern. In the period 2001-2010, a total of 26 collisions between ship and platforms were reported on the Norwegian Continental Shelf. According to Kvitrud (2011) the leading causes of these accidents are concerned with lack of safety culture, too sophisticated equipment, and inadequately trained crew. Although the number of reports regarding ship-installation impacts in the offshore wind energy industry are limited, it is reasonable to assume that, due to the same operating conditions and procedures, the same causes can lead to a collision between service vessels and FOWTs. According to *Caithness Windfarm Information Forum* (2020), an average number of 49 accidents per year took place from 2000 to 2004 in the UK's wind farms. Between 2005 and 2009, this number increased to 109, and from 2015 to 2019, the number was 210 accidents per year. Among the causes behind these accidents were fire, structural failure, and ship collisions.

On 21st September 2003, a floating dock threatened the turbines of an offshore wind farm in Denmark (Moulas, M. Shafiee, and Mehmanparast 2017). However, the vessel was reconnected so that no accident occurred. Another incident occurred in 2006, where a jack-up barge collided with an OWT in the Scroby Sands wind farm (ibid.). The result of this accident was that vital maintenance works were interrupted, and parts of the turbine blade were broken.

The standards for floating offshore wind turbines states that the characteristic loads from ship impacts shall be taken from the maximum authorized service vessel that can approach

the installation. According to Dai et al. (2013), typical service vessel operations may lead to collision impacts:

- Service vessel approaching the FOWT
 - Service vessel fails to stop and hits the FOWT in high speed
 - The service vessel misjudges the FOWT and hits it at low speed.
- Service vessel is alongside the FOWT performing a task
 - Vessel loses motor power or dynamic positioning system fails, causing the vessel to drift into the FOWT due to winds and waves. The speed depends on the current sea state.

The likelihood of occurrence depends on several factors. Among these are the type of ship, shipping traffic, navigation routes, and layout of the wind farm (Christensen, Andersen, and Pedersen 2001). The type of collision also influences the likelihood, which can be either powered or drifting collision. Based on this, three collision scenarios are plausible:

1. Head-on collision
2. Maneuvering collision
3. Drifting collision

4.1 Consequences

The consequences of ship collisions can range from minor to major, i.e., from maintenance work to the collapse of the OWT support (Bela et al. 2017). Structural damage, environmental impacts, and personnel injuries are three domains often used for evaluating the consequences (Presencia and Mahmood Shafiee 2018). Table 4.1 display the possible impact a ship collision may have on an operating wind turbine.

Consequence	Description
Not significant	No influence on operation
Considerable	Not significant damage from collision, but turbine stops operating
Serious	Serious damage due to collision
Catastrophic	Excessive damage of wind turbine. Parts of nacelle falls onto ship deck.

Table 4.1: Magnitude of consequence of ship collision (Presencia and Mahmood Shafiee 2018)

Damage analysis of ship-wind turbine collisions is a recent topic in the offshore wind industry, and the most critical factors affecting the magnitude of damage are (Moulas, M. Shafiee, and Mehmanparast 2017):

1. Technical specifications of the ship. Such as its tonnage, stiffness, and average speed.
2. Structural properties of wind turbine and foundation. Such as strength, toughness, and brittleness.

Evaluating the consequences of a ship-wind turbine collision in the three domains mentioned needs to highlight both the effects on the ship and wind turbine. According to Moulas, M. Shafiee, and Mehmanparast (ibid.) a classification given in Table 4.2 is reasonable.

Consequence	Damage to wind turbine	Damage to ship
Economic	Reputation damage, loss of assets, repair cost and loss of electricity production	Reputation damage, loss of assets repair cost and loss of revenues
Environmental	Discharge of oil spills. E.g gearbox oil	Discharge chemical substance
Health and Safety	Injuries or fatalities on maintenance crew	Injuries or fatalities ship crew

Table 4.2: Potential impacts according to Moulas, M. Shafiee, and Mehmanparast (2017)

Large accelerations of the nacelle can cause loss of electricity production. According to Bela et al. (2017) the turbine generator is sensitive to high accelerations, and limiting it to 0.2-0.3 g is suggested. Exceeding the critical level is potentially dangerous. Biehl and Lehmann (2006) performed collision analyses on different bottom-fixed wind turbine

foundations, and collapse of the structures is a general concern. Investigation of various ship collisions resulted in observations of collapse in both the ship's direction and away from the ship.

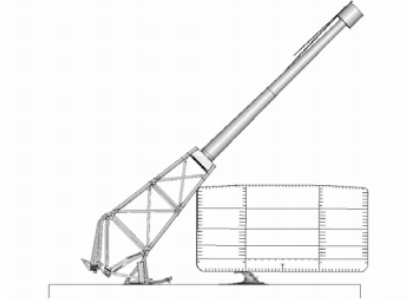


Figure 4.1: Collapse OWT (Biehl and Lehmann 2006)

Amdahl and Holmås (2011) also examined the effect of high energy collisions on OWTs, and found that when the foundations were fixed to the seabed, the turbine could collapse towards the ship. The rotor and nacelle would then fall on the ship deck. For that matter, the preferred event is that the tower falls in the drift direction or over to the other side of the ship.

In this thesis, ship collisions with a floating offshore wind turbine are evaluated, and comparing the results obtained for OWTs to FOWTs is not straight forward. Interaction with mooring lines influence the response, and failure of one or more of these lines is a consequence that also should be considered.

Chapter 5

FEA using LS-DYNA and USFOS

Ship collision with floating offshore wind turbines will induce large structural deformations and displacements, so nonlinear material behavior is expected. Nonlinearity is associated with nonlinear stress-strain relationships, large deformations, and changing boundary conditions.

The ship collision analyses in this thesis are executed in the simulation programs USFOS and LS-DYNA, and this chapter highlights NFEA using these tools.

5.1 USFOS

In this section, a summary of the theory behind USFOS is presented. Further information can be found in *USFOS Getting Started* (2001).

USFOS is a computer program that is developed for nonlinear static and dynamic analysis of structures, and it includes both nonlinear geometry and material properties. Formulation of beam models allows for coarse modeling of the structures while still obtaining a good accuracy in the results.

USFOS follows an updated Lagrange formulation, often referred to as material description. The element stiffness relations are in this formulation first determined in a local coordinate system that follows the structure during deformation. That means that the reference system must be updated during deformation, and the updated Lagrange formulation uses the configuration from the previous time step for the stiffness relationships. The nonlinear geometrical effects are therefore accounted for by continuously changing the transformation matrices. Further, USFOS uses Green strain formulation, which means that the beam elements are valid for large displacements and moderate strains. The nonlinear strain relationships accurately represent element behavior, and both membrane effects and column buckling are included.

$$\varepsilon_x = u_{,x} + \frac{1}{2}u_{,x}^2 + \frac{1}{2}v_{,x}^2 + \frac{1}{2}w_{,x}^2 \quad (5.1)$$

The main idea behind the program is to use one finite element per physical element of the structure (*USFOS Getting Started* 2001). Plasticity is modeled by hinges occurring at element ends or midspan, and in the latter case, the original element is subdivided into two sub-elements.

Incremental procedures introduce incremental stiffness and in USFOS this is obtained by using interpolation functions. The element displacements are calculated by:

$$\begin{aligned} u(x) &= \phi^T Q_u \\ v(x) &= \phi^T Q_v \\ w(x) &= \phi^T Q_w \end{aligned} \quad (5.2)$$

The shape functions, ϕ , are the exact solution of the 4th order differential equation for a beam-column and is often denoted Livesley functions.

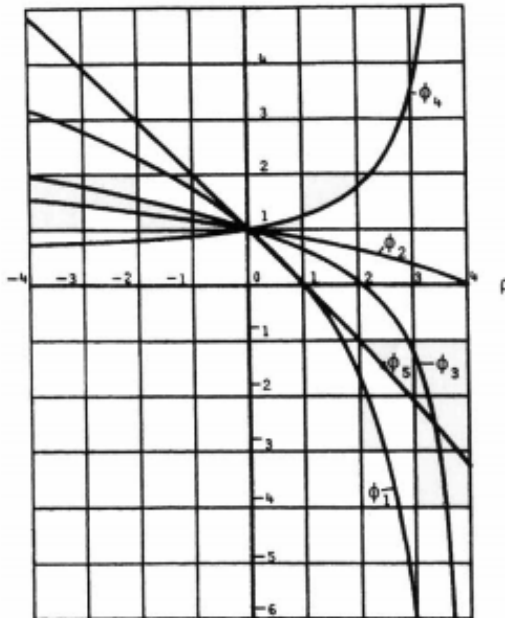


Figure 5.1: Livesley functions (Moan 2003)

5.2 LS-DYNA

LS-DYNA is a general-purpose finite element program developed for large deformation static and dynamic response analyses (*LS-DYNA Theory Manual* 2019). The solution methodology for the dynamic equilibrium equation is based on explicit time integration.

$$\mathbf{M}\ddot{\mathbf{r}} + \mathbf{C}\dot{\mathbf{r}} + \mathbf{K}\mathbf{r} = \mathbf{R}(t) \quad (5.3)$$

The time integration method is denoted explicit as the displacements, \mathbf{r} , at the new time step are only dependent on the displacements, velocities, and accelerations of previous time steps.

$$\mathbf{r}_{i+1} = f \{ \mathbf{r}_i, \dot{\mathbf{r}}_i, \ddot{\mathbf{r}}_i, \mathbf{r}_{i-1}, \dot{\mathbf{r}}_{i-1}, \ddot{\mathbf{r}}_{i-1}, \dots \} \quad (5.4)$$

In LS-DYNA the semi-discrete equations of motion at a given time instant n is given by:

$$\mathbf{M}\mathbf{a}^n = \mathbf{P}^n - \mathbf{F}^n + \mathbf{H}^n \quad (5.5)$$

Where

- \mathbf{M} Diagonal mass matrix.
- \mathbf{a}^n Acceleration vector at time n .
- \mathbf{P}^n External and body force loads at time n .
- \mathbf{F}^n Stress divergence vector at time n .
- \mathbf{H}^n Hourglass resistance at time n .

The central difference method is used to advance to the next time step.

$$\mathbf{a}^n = \mathbf{M}^{-1} (\mathbf{P}^n - \mathbf{F}^n + \mathbf{H}^n) \quad (5.6)$$

$$\mathbf{v}^{n+1/2} = \mathbf{v}^{n-1/2} + \mathbf{a}^n \Delta t^n \quad (5.7)$$

$$\mathbf{u}^{n+1} = \mathbf{u}^n + \mathbf{v}^{n+1/2} \Delta t^{n+1/2} \quad (5.8)$$

$$\Delta t^{n+1/2} = \frac{(\Delta t^n + \Delta t^{n+1})}{2} \quad (5.9)$$

The global nodal velocity and displacement vectors are \mathbf{v} and \mathbf{u} , respectively. The geometry is updated by adding the displacement increments to the initial geometry:

$$\mathbf{x}^{n+1} = \mathbf{x}^0 + \mathbf{u}^{n+1} \quad (5.10)$$

Explicit methods are conditionally stable, which indicates that the time steps have to be small. The highest natural frequency bounds the stability of the central difference method:

$$\Delta t \leq \frac{2}{\omega_{\max}} \quad (5.11)$$

To determine the maximum natural frequency of an element, the time step Δt must be short so that no information propagate across multiple elements per time step (Moan 2003). Based on this, the maximum time step is limited by the characteristic length of the element, λ_e , and the acoustic wave speed, c .

$$\Delta t = \frac{\lambda_e}{c} \quad (5.12)$$

$$c = \sqrt{\frac{E}{\rho(1 - \nu^2)}} \quad (5.13)$$

There exist three different methods for determining the characteristic length in LS-DYNA. The default option is given in Equation 5.14 (*LS-DYNA Theory Manual* 2019).

$$\lambda_e = \frac{(1 + \beta)A_s}{\max(L_1, L_2, L_3, (1 - \beta)L_4)} \quad (5.14)$$

where $\beta = 0$ for quadrilateral shell elements, A_s is the area, and L_i represents the sides that define the shell elements.

5.2.1 Shell elements

LS-DYNA has multiple options for element types. The default option for shell elements is Belytschko-Lin-Tsay shell elements. In this Master thesis, two different ship models are used in the collision analyses, and that is a supply ship bow model and a ship side model. The first model uses Belytschko-Lin-Tsay shell elements, while the latter model uses Hughes-Liu shell elements. In this section, a brief introduction to these shell elements is given. Detailed description can be found in *LS-DYNA Theory Manual* (2019).

Co-rotational and velocity strain formulation are the basis for the Belytschko-Lin-Tsay element (ibid.). The first formulation separates the deformation displacements, which give rise to strain energy, from the rigid body displacements. This is usually accomplished by comparing a reference configuration to the instantaneous configuration. The reference configuration is normally taken as the configuration at the previous time step. The Belytschko-Lin-Tsay shell element is the default option in LS-DYNA due to its computational efficiency. For a shell element with five through-thickness integration points, this element formulation requires around 80 % less mathematical operations than the Hughes-Liu element.

The Hughes-Liu element formulation was the first shell element implemented in LS-DYNA, and these elements allow for the treatment of finite strains. It includes finite transverse strains, but the CPU efficiency is low compared to Belytschko-Lin-Tsay elements.

Finite element models in USFOS

The collision analyses include a 10 MW turbine on the OO Star Wind Floater foundation. Global analyses are performed using USFOS, while the local analyses are done in LS-DYNA. Finite element models are therefore established in both these computer programs, and this chapter highlights the principal dimensions and modeling procedures in USFOS.

6.1 10 MW turbine

The light rotor project (Bak et al. 2013) is a project with the main objective to optimize blade design for wind turbines. The project is a cooperation between DTU Wind Energy and Vestas, and in relation to this, the DTU 10 MW Reference Wind Turbine has been established. The finite element model for the turbine in this thesis is based on the reference turbine, and some of the main characteristics are summarized in Table 6.1.

Parameter	DTU 10 MW RWT	
Rotor Diameter	178.3	[m]
Hub Diameter	5.6	[m]
Hub Height	119.0	[m]
Nacelle Mass	446 036	[kg]
Tower Mass	628 442	[kg]
Hub Overhang	7.1	[m]
Shaft Tilt Angle	5	[deg]
Rotor Precone Angle	-2.5	[deg]
Maximum Rotor Speed	9.6	[rpm]
Rated Wind Speed	11.4	[m/s]

Table 6.1: Key parameters 10MW Reference Wind Turbine

The turbine blades are modeled based on a geometric description provided in an excel sheet. The blades have a prebend, and in order to obtain sufficient accuracy, a total of 27

nodal points are specified for each blade. In USFOS, the basic structural unit used is the two-node beam element, creating 26 beam elements for each of the blades.

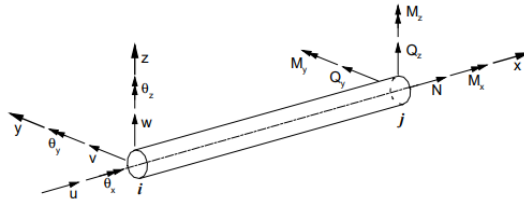


Figure 6.1: Three dimensional beam element in USFOS (*USFOS USER'S MANUAL-MODELLING* 1999)

It is convenient to consider the blade as composed of a discrete number of elements, each with specific cross-section, structural properties, and mass. The user input GENBEAM is used to assign material properties to different elements. Along the blade, the angle of attack varies, and one of the reasons is that the individual blade segments are normally twisted. In general, the elements closest to the hub have the most significant structural twist. In USFOS, this is accounted for by defining a local coordinate system for the different sections so that the individual elements are rotated according to the reference model. The structural twist of the beam elements is displayed in Figure 6.2.

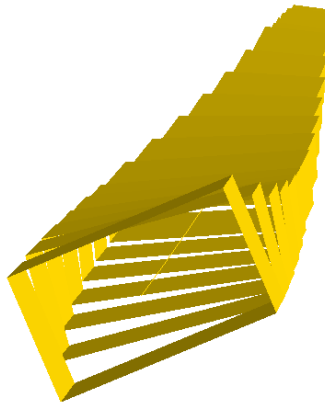


Figure 6.2: Blade model in USFOS with structural twist

All the individual elements are aerodynamic airfoils that create lift and drag forces that act in the aerodynamic center of the airfoil. These forces are orientated perpendicular to and along the direction of the inflow, respectively. A total of 10 different foil profiles are used to establish each blade.

$$F_D = \frac{1}{2} \cdot \rho \cdot W^2 \cdot C_D \cdot A \quad (6.1)$$

$$F_L = \frac{1}{2} \cdot \rho \cdot W^2 \cdot C_L \cdot A \quad (6.2)$$

The drag and lift coefficient for the airfoils depends on the angle of attack. For all the different airfoils, 2D data is given for these coefficients at multiple different attack angles. By calculating the relative velocity and account for the structural twist of the blade elements, the various attack angles are determined.

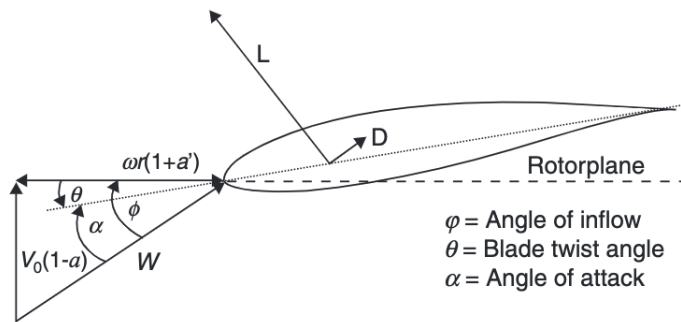


Figure 6.3: Velocity and forces on a blade segment (Brøndsted and P.L Nijssen 2013)

The relative velocity, W , is calculated by the rated wind speed, V_0 , and rotational speed, ωr , on the blade segment. The drag and lift forces are then computed by using Equation 6.1 and 6.2, respectively.

Although the forces are calculated for each blade segment, they are included in USFOS as nodal forces. The drag and lift forces are calculated with reference to the local coordinate system for the blade segments. The two force contributions are merged into one and modeled to act in the same global direction as the incoming wind. The reason for this modeling procedure is that the wind field is not modeled in USFOS, so the forces occurring in the global direction of the wind field are the most important. This will help determine if the turbine blades will hit the tower during a ship collision impact.

The ship collision analyses shall include the 10 MW turbine in both parked and operating conditions. The ability to rotate the turbine blades is therefore essential. This is modeled by a zero-length spring, which is created at the rotor connection. This spring has no stiffness in the torque degree of freedom while infinite stiffness in the other five. A torque moment is applied at the rotor and adjusted until the maximum rotor speed defined in Table 6.1 is achieved. Rotor speed of 9.6 rpm corresponds to a nodal velocity of $1 \frac{rad}{s}$ at the rotor center.

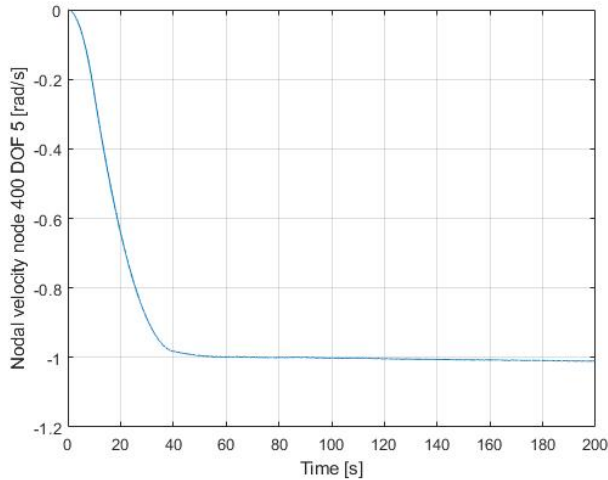


Figure 6.4: Rotational velocity at rotor centre

Connecting all the blades to the rotor is modeled by tubular elements with high yield capacity. The same material properties apply for the member connecting the rotor to the turbine tower. The reason for increasing the yield strength is that large stresses occur when rotation is applied, and plasticity should be prevented. Multiplying the yield strength for regular steel, i.e., 350 MPa, by 1000 gives sufficient strength. The turbine tower is subdivided into ten elements with regular steel properties and a density of $8500 \frac{kg}{m^3}$ to account for secondary structures.

Property	Value	
Young's modulus	2.1E+11	[MPa]
Yield strength	350	[MPa]
Density	7850	$[\frac{kg}{m^3}]$

Table 6.2: Regular steel properties

6.1.1 Tower clearance

The risk of blades hitting the turbine tower is dealt with by having sufficient tower clearance. Modern wind turbines have tilted shaft, cone angle, and prebend of the blades that all increases the distance between the blade tips and tower. The tower clearance for the 10 MW DTU RWT is 18.26 m when loading of the blades are not accounted for (Bak et al. 2013).

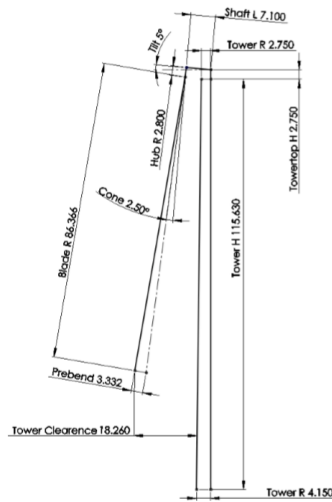


Figure 6.5: Tower clearance description according to Bak et al. (2013)

Prebend of the blades is included in USFOS. However, tilt and cone are not modeled. The 10MW RWT has a tilted shaft with length 7.1 m positioned at 2.75 m above the top of the tower. In USFOS, the shaft is horizontal with a length of 6.25 m and is located at the top of the tower center. The total tower clearance in USFOS is therefore limited to 5.7 m at the location where the blade tip can hit the tower. This clearance is drastically lower. During a ship collision, if the relative distance between the tower and the blade tip in USFOS is below 5.7 m, the modeled clearance is sufficient. Additionally, the model is considered conservative with respect to the reference turbine, so if the clearance in USFOS is valid, the structure is considered to prevent the blades from hitting the tower in real life.

6.1.2 Model verification

The wind turbine model must be verified so that the results obtained from the collision analyses are useful. The verification consist of computing the natural frequencies for the isolated blades and the turbine as values for these quantities are given in the description of the 10 MW reference turbine (ibid.).

Natural frequency for the blades

Table 6.3 gives information about the four first eigenmodes for the isolated blade. The deviation in results is small, which indicates that the blade model will give sufficient accuracy. For higher eigenmodes than the ones presented, the deviations increase. However, these are considered as less important as the lowest ones will govern the behavior. One of the topics for this thesis is that the beam model of the blades shall be established with the correct flexibility, and similarity in natural frequencies is considered to validate this.

Mode	Natural frequency [Hz] DTU	Natural frequency [Hz] USFOS model	Deviation [%]
1st flap mode	0.61	0.61	0.0
1st edge mode	0.93	0.91	2.15
2nd flap mode	1.74	1.81	-3.87
2nd edge mode	2.76	2.85	-3.26

Table 6.3: Natural frequencies for the isolated blade

The next verification procedure is to connect the three turbine blades to the tower. The eigenvalue analysis is performed on a turbine model that is fixed at the bottom of the tower, so it will essentially be a turbine on a fixed foundation. The assembled structure in USFOS is displayed in Figure 6.6.

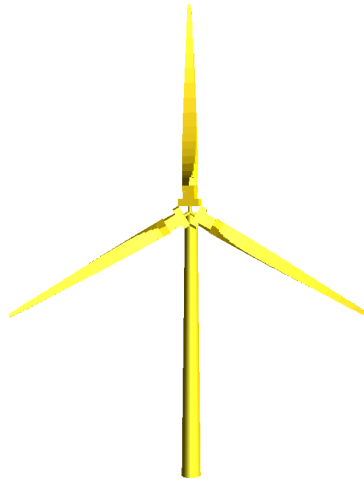


Figure 6.6: Reference turbine USFOS

Table 6.4 contains information on the natural frequencies of the whole turbine. As seen, the deviations are limited.

Mode	Natural frequency DTU [Hz]	Natural frequency USFOS model [Hz]	Deviation [%]
1st Tower side-side mode	0.25	0.26	-4
1st asymmetric flap with jaw	0.55	0.54	1.82
1st asymmetric flap with tilt	0.59	0.58	1.70
1st collective flap mode	0.63	0.63	0.0

Table 6.4: Natural frequencies for the whole turbine

Based on these checks, the wind turbine model is considered to be verified. For the assem-

bled structure, the blades and rotor mass are placed around 6 meters from the tower center by a horizontal beam element. In reality, the shaft is tilted by 5° as well as the rotor has a precone angle of 2.5° . Both these effects will influence the natural frequency of the tower as the mass center will be shifted.

6.2 OO-Star Wind Floater

The OO-Star Wind Floater is a concept developed by Dr. techn. Olav Olsen AS. It is a part of the LIFES50+ project, which has the primary goal of developing cost-effective solutions for floating substructure design for 10 MW wind turbines (*Lifes50plus - Innovative floating offshore wind energy* 2020).

The semi-submersible platform consists of four columns mounted on a star-shaped pontoon built in post-tensioned concrete (W. Yu, Müller, and Lemmer 2018). All the columns consist of a cylindrical upper part and a tapered lower part where the distance between the central column and the outer is 37 m (ibid.). Horizontal pontoon elements connect the columns with a width of 16 m and a height of 7 m. Underneath the pontoons there is a slab that adds 0.5 m to each side. At the tower base interface, the diameter of the central column is 12.05 m. The tapered section underneath increases linearly in diameter to 16.2 m at the pontoon intersection. At the top, the outer columns have a diameter of 13.4 m and at the tapered section, the diameter increases to 15.8 m at the pontoon interface. Finally, there are three circular heave plates underneath the outer columns with a diameter of 22.8 m. The geometrical properties of OO-Star Wind Floater are displayed in Figure 6.7.

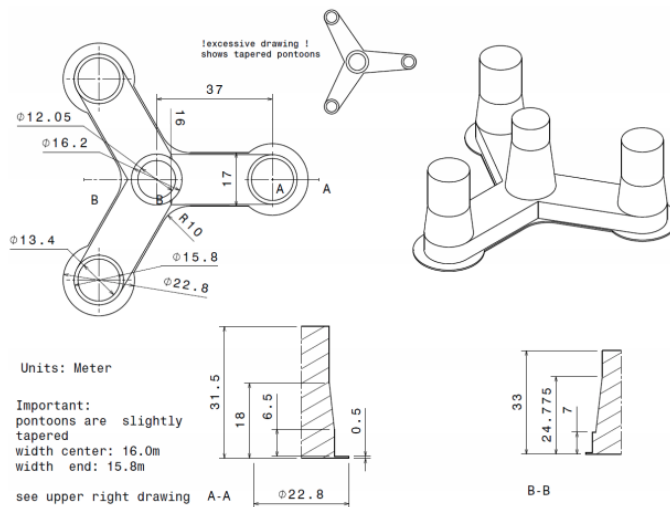


Figure 6.7: Main dimensions OO-Star Wind Floater 10 MW (W. Yu, Müller, and Lemmer 2018)

In Table 6.5 important structural properties are listed, and Figure 6.8 defines the coordinate system applied for the structure.

Property	Unit	Value
Substructure mass excluding tower and mooring	[kg]	2.1709E+07
Centre of Mass (CM) below MSL	[m]	15.225
Roll inertia about CM	[kg m ²]	9.43E+09
Pitch inertia about CM	[kg m ²]	9.43E+09
Yaw inertia about CM	[kg m ²]	1.63E+10
Interface with tower above MSL	[m]	11.0
Displaced water volume	[m ³]	2.3509E+04
Centre of Buoyancy below MSL	[m]	14.236
Draft at equilibrium with moorings	[m]	22.0

Table 6.5: Platform parameters for OO-Star Wind Floater (W. Yu, Müller, and Lemmer 2018)

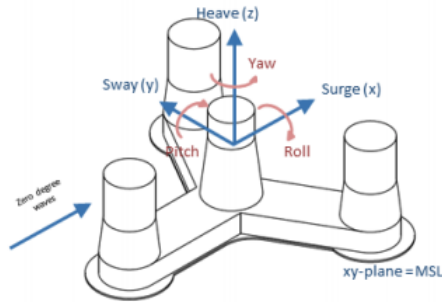


Figure 6.8: Coordinate system OO-Star Wind Floater 10 MW (W. Yu, Müller, and Lemmer 2018)

Similar to the turbine model, the OO-Star Wind Floater is modeled by beam elements. The original floater with properties given in Table 6.5 is built in concrete with ballast to stabilize it. The model in USFOS does not include ballast. In order to keep the installation stable, the material density of the floater is increased. This procedure causes iteration until sufficient accuracy is reached. The starting point is to assemble the 10 MW reference turbine onto the floater. A Stoke wave with zero height is added at the equilibrium draft of 22 m for the floater. The buoyancy force is given by the displaced volume at this surface level, so the weight is changed to obtain equilibrium. The fact that the reference turbine earlier has been verified according to specifications makes it reasonable to change only the weight of the floater in this process. The floating structure is subdivided into three sections with different densities so that the metacentric height more efficiently can be influenced. Gravity and buoyancy are applied at the same time instant, and the fluctuations in the z-coordinate at the tower intersection is evaluated. The goal is to keep these fluctuations as close to zero as possible.

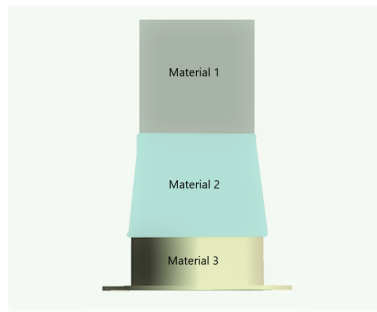


Figure 6.9: Material density division

Figure 6.10 display the fluctuations in z-direction around zero for the nodal coordinate at the tower intersection when the mooring lines are connected. The fluctuations are low, which indicates that the buoyancy force and structural mass force are close to equilibrium. The response of the floater is considered to have sufficient accuracy.

In order to keep the floating structure intact the Young's modulus and yield stress needs to be increased. The latter modifications are considered as less important as the main considerations in USFOS are the global responses of the structure. Local effects on the floater are to be evaluated in LS-DYNA. The final material properties for the floater are given in Table 6.6.

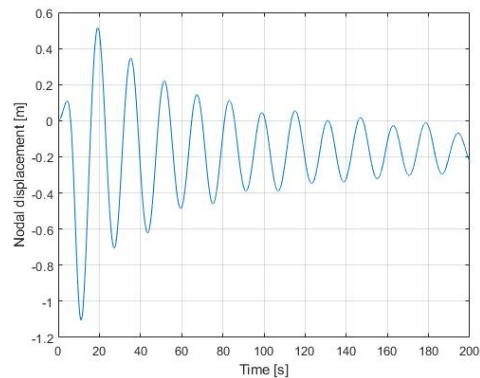


Figure 6.10: Nodal displacement at tower intersection in global z-direction

Property	Unit	Material 1	Material 2	Material 3
Young's modulus	[Pa]	20E+11	20E+11	20E+11
Yield stress	[Pa]	20E+08	20E+08	20E+08
Density	[$\frac{kg}{m^3}$]	3100	3130	17700

Table 6.6: Material properties OO-Star Wind Floater

Mooring System

The mooring system on OO-Star Wind Floater is a catenary system with three mooring lines where the horizontal angle between two chains is 120° . At each line there is a clumped mass of 50 tonnes attached, separating the line in two. The layout is shown in Figure 6.11. The segment connected to the floater is 160 m long and the lower segment is 543 m long (W. Yu, Müller, and Lemmer 2018). Some of the main parameters of the mooring system are summarized in Table 6.7.

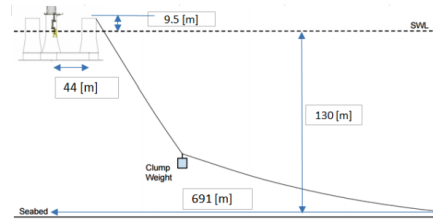


Figure 6.11: Mooring system (W. Yu, Müller, and Lemmer 2018)

Property	Unit	Value
Number of lines	[-]	3
Angle between adjacent mooring lines	[deg]	120
Total mass clump weight	[kg]	50 000
Upper segment length, unstretched	[m]	118
Lower segment length, unstretched	[m]	585
Location of fairleads above MSL	[m]	9.5
Initial position of clump mass below MSL	[m]	90.45
Equivalent weight in water	[N/m]	3200.6
Pre tension	[N]	1.67E+06
Extensional stiffness EA	[N]	1.506E+09
Hydrodynamic added mass coefficient	[-]	0.8
Hydrodynamic drag coefficient	[-]	2.0
Effective hydraulic diameter of chain	[m]	0.246

Table 6.7: Mooring system properties (W. Yu, Müller, and Lemmer 2018)

The mooring lines are modeled according to the properties, and three nodal points are assigned for each line. The three nodes are located at the fairlead, clump mass, and sea bottom. Beam elements with circular cross-sections are used to connect the nodes. The mooring line's density is $7850 \frac{kg}{m^3}$ with a diameter of 0.488 m and a thickness of 0.04 m. The equivalent weight in water is used to determine the buoyancy diameter to 0.44 m. Further, the extensional stiffness is obtained by modifying Young's modulus based on the cross-sectional area used for the mooring lines. The added mass and drag coefficients are multiplied by a factor of 0.5 as the hydraulic diameter in USFOS is larger than specified in Table 6.7.

The mooring system's layout and weight gives a pretension in the mooring lines of $1.67\text{E}+06$ N. Subdividing the segments into smaller elements is essential to obtain horizontal and vertical equilibrium of the clump weights. Therefore, the USFOS command REFINE is used to subdivide each of the segments into ten smaller elements. The initial length of the lower segment is 543 m, but in USFOS, this is modified to be 230 m long. Additionally, normal forces and springs at the nodes on the sea surface are applied to get the correct shape and pretension of the mooring system. These modifications are considered valid as the correct pretension and natural frequency are obtained with this layout. Consultation with the supervisor has also strengthened the validity of this modification. The mooring system in USFOS is displayed in Figure 6.12 and the pretension in Figure 6.13a.

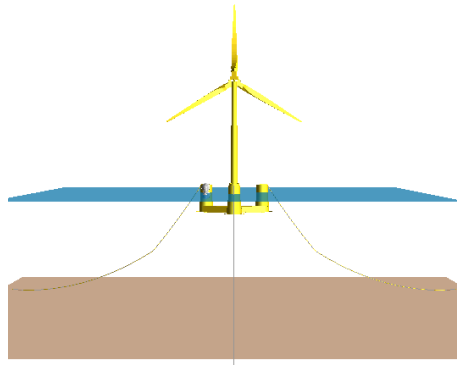
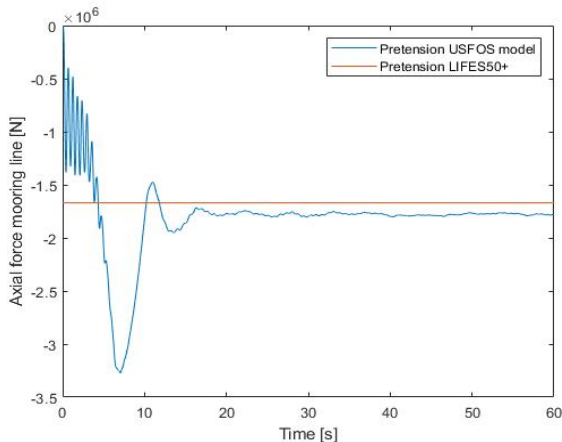
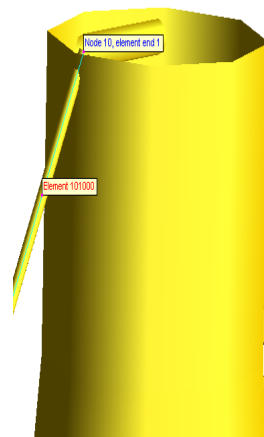


Figure 6.12: Mooring system model in USFOS



(a) Pretension in element 101000



(b) Mooring element 101000

Figure 6.13: Pretension in mooring line

From the figure, it is clear that the tension at the fairled stabilizes after around 20 seconds,

and the result is identical for all three mooring lines. The pretension is slightly higher than given in the LIFES50+ document. However, the modifications and results are considered to have sufficient accuracy to represent the mooring system properly.

6.3 Assembled model

The assembled model is displayed in Figure 6.12. All the elements in this model have Rayleigh-damping:

$$\mathbf{C} = \alpha_1 \mathbf{M} + \alpha_2 \mathbf{K} \quad (6.3)$$

where \mathbf{M} denote the mass matrix and \mathbf{K} the stiffness matrix of the system. The model in USFOS is only proportional to the stiffness term, i.e., α_1 is set to zero. In general this means that the higher mode shapes are damped out. However, these damping terms will be of minor importance, as most of the damping comes from the hydrodynamic mass and drag forces (*USFOS Gettin Started* 2001). The hydrodynamic added mass and drag coefficients for the mooring system is based on properties given in the LIFES50+ document (W. Yu, Müller, and Lemmer 2018). For the rest of the structure, these coefficients are determined based on elevation above and below MSL:

Elevation [m]	Added mass coefficient [-]	Drag coefficient [-]
5	1.6	0.65
0	1.6	0.65
-5	1.2	1.05
-40	1.2	1.05

Table 6.8: Added mass and drag coefficients in USFOS

The assembled model oscillates significantly using these coefficients, so more damping of the FOWT is achieved by increasing the drag coefficient for the three horizontal pontoon elements to $0.65 \cdot 20$. The mass coefficient for these three elements are increased to 1.8, meaning that the added mass of these elements are 80 % of the mass.

6.4 Model verification

The overall system is verified based on data from the LIFES50+ document where properties are presented, among these are the natural frequencies in different directions. From the defined coordinate system in Figure 6.8, the wind load acts in the negative surge direction. The total force acting on the three blades is concentrated at the rotor connection, and a free decay test is carried out. This test is used to determine the natural period in pitch.

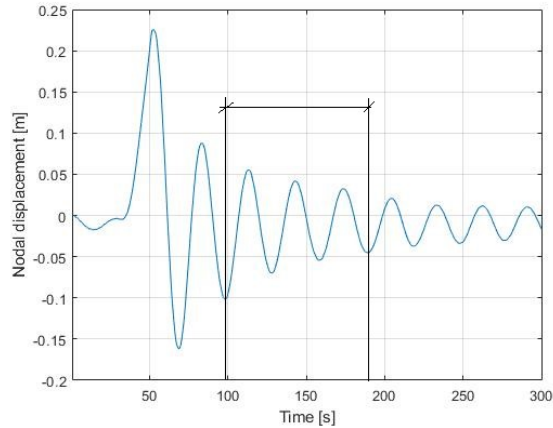


Figure 6.14: Nodal displacement at intersection between turbine tower and OO-Star

The nodal displacement at the tower connection in pitch is extracted from USFOS, and the natural period is calculated by evaluating an interval from 100 to 200 seconds. In this region, clear damping of the response is present, and the decrease is approximately linear. That makes the interval reasonable to use, and the damped natural period in pitch is given in Table 6.9.

Natural period in pitch from USFOS [s]	Natural period in pitch from Lifes50+ [s]
30.2	31.25

Table 6.9: Natural period in pitch for OO-Star Wind Floater

The decay test is carried out with the mooring lines attached. This is in accordance with the system property given in the LIFES50+ document. The deviation in the natural period is considered insignificant.

Additional validation is carried out by evaluating the center of gravity and buoyancy for the assembled FOWT. All these properties are given in the LIFES50+ document, though it is split into separate tower properties and floater properties. The parameters necessary are summarized in Table 6.10

Property	Unit	Value
Total mass of tower	[kg]	1.257E+06
Vertical centre of mass (above MSL)	[m]	49.8
Total mass of substructure (excl. tower, mooring)	[kg]	2.1709E+07
Centre of mass substructure (below MSL)	[m]	15.225
Centre of buoyancy substructure (below MSL)	[m]	14.236
Displaced water volume	[m ³]	2.3509E+04

Table 6.10: Tower and platform parameters (W. Yu, Müller, and Lemmer 2018)

The combined substructure and wind turbine have a centre of gravity located at:

$$CoG_{FOWT} = \frac{2.17E + 07 \cdot (-15.2) + 1.26E + 06 \cdot 49.8}{2.17E + 07 + 1.26E + 06} = -11.7[m] \quad (6.4)$$

The center of gravity and buoyancy are compared to results obtained in USFOS.

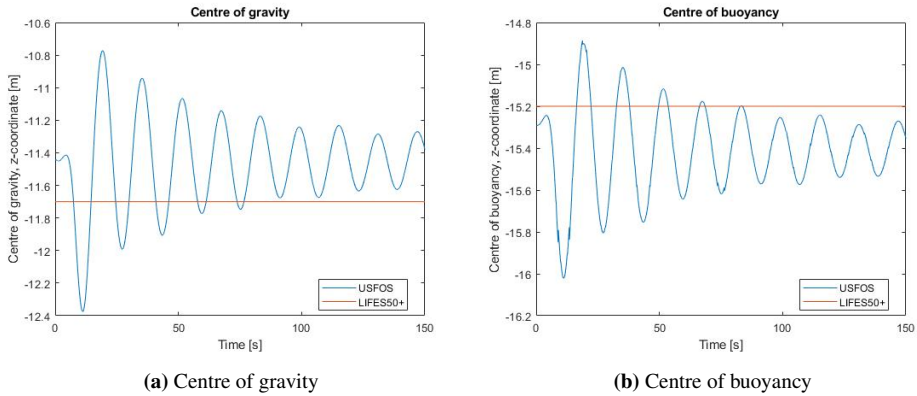


Figure 6.15: CoG and CoB USFOS

From Figure 6.15, it is clear that the center of gravity is higher for the USFOS model than compared to the LIFES50+ document. The buoyancy centre is lower in USFOS, which indicates that the buoyancy force is larger in USFOS than for the real model. The displaced volume of OO-Star Wind Floater substructure is $2.35E+04 \text{ m}^3$. This gives a buoyancy force of 236 MN. The buoyancy force from USFOS is displayed in Figure 6.16.

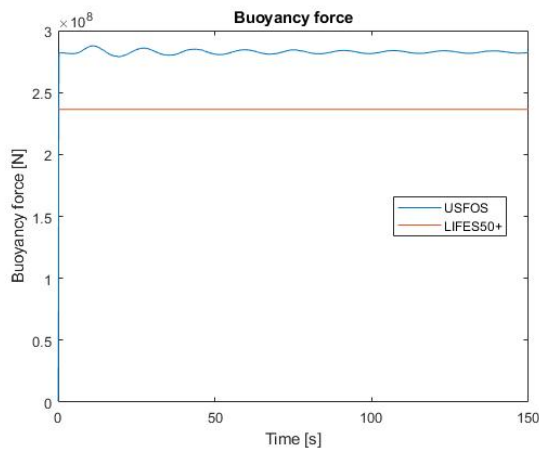


Figure 6.16: Buoyancy force USFOS vs LIFES50+

As suspected, the buoyancy force for the USFOS model is higher than for the real structure. The total weight of the structure in USFOS can be collected in the OUT-file, and from this the total weight is $2.88E+07$ kg instead of $2.3E+07$ kg which is correct in terms of the LIFES50+ document. Following Archimedes' principle, the FOWT sinks in the water until the buoyancy force equals the weight. For that matter, the buoyancy force that is needed in order to achieve equilibrium is around 280 MN, and this corresponds well to Figure 6.16.

The distance between CoG and CoB in USFOS is larger than the real model, meaning that the metacentric height (GM) is lower for the model in USFOS. The lower metacentric height is expected to influence the natural period in pitch to be larger than anticipated in the LIFES50+ document. However, it is lower. The reason for this is difficult to determine. Possible explanations includes difference in added mass and stiffness of the mooring system. On the other hand, the difference in natural period between USFOS and the LIFES50+ document is insignificant.

6.5 Ship collision model

The ship impact is modeled in USFOS by using a spring system containing both linear and nonlinear springs. The ship is modeled as a mass point connected to the nonlinear spring. Collision by bulbous bow and ship side are considered in this thesis, and this gives two different spring systems. Figure 6.17 displays the collision system for bow impact, and Figure 6.18 displays the system used for ship side impact. The spring systems' location is based on structural properties for the colliding ship, which is UT745 Platform Supply Vessel.

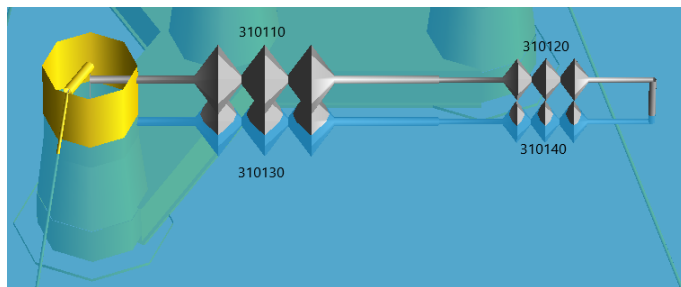


Figure 6.17: Collision system for bow in USFOS

Impact by bulbous bow is split into two contributions, one from the forecastle and one from the bulb. The nonlinear spring element for the forecastle is *310120*, and it is located at the center of the forecastle. Element *310140* represents the bow, and this spring is located in the center of the bulb. Attached to the nonlinear springs are the linear spring elements *310110* and *310130* for the forecastle and bulb, respectively.

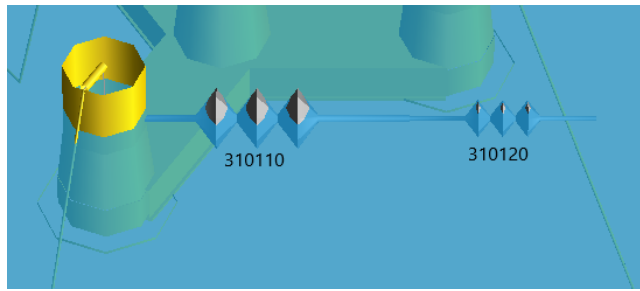


Figure 6.18: Collision system for ship side in USFOS

Impact by ship side is modeled by one nonlinear spring, and this is element *310120* in Figure 6.18. The location is assumed to be in the center of the ship side model.

Linear springs

It is desirable that the ship disconnects from the floating structure after the collision. This is achieved by modelling compression springs, and with reference to Figure 6.17 and 6.18, the linear springs are element number *310110* and *310130* for bow impact and *310110* for side impact. These springs are given large stiffness in compression, i.e., $1E+08$ N/m , and zero stiffness in tension. This ensures that no energy is dissipated in the springs and that the spring force is close to zero as the ship gets pushed back by the resistance of the floater.

Nonlinear springs

The nonlinear springs are element number *310120* and *310140* for bow impact and *310120* for side impact. These springs contain the force-displacement curves for the ship. The stiffness is provided by individual points in these curves. Attached to these springs is the ship mass that is modeled as a vertical column with a mass magnitude of 7.5 Mkg. The hydrodynamic added mass is included in the ship mass, and with reference to Chapter 3, the added mass contribution is 10% and 40% of the total mass for bow and side-impact, respectively. The minimum value of ship mass for an impact given in the NORSOK standard is specified as 10,000 tonnes. Hence, the ship considered for this analysis is nonconservative with respect to NORSOK.

The ship collision nodes are free to translate in the horizontal plane, i.e., translation in x - and y -direction is free. The other four directions are fixed. It is interesting to evaluate ship impacts in multiple different directions, so the nodal points are modified for different scenarios.

The force-displacement curves used as input for the nonlinear springs are established using LS-DYNA. These curves need to be created before global response of the structure in USFOS is investigated.

Local analyses in LS-DYNA

The ship collision model for the global analyses in USFOS described in section 6.5 uses force-displacement curves for the ship as input. These curves are established in LS-DYNA. The impact scenarios that are considered are head-on collision and sideways impact of the OO Star Wind Floater. This chapter provides description of the different models, analysis setup and results from the LS-DYNA analyses. Further, high strength ship bows and strengthened ship sides may induce excessive punching shear damage on the floating structure. This issue will also be investigated and the danger will be evaluated.

7.1 Design ship

In the design against accidental ship collision the maximum authorized service vessel that can approach the FOWT shall be considered. The design ship chosen in this thesis is the UT 745 Platform Supply Vessel as detailed finite element models have been provided. Main data for this ship is summarized in Table 7.1.

Parameter	Value
Length overall [m]	82.5
Depth [m]	7.6
Draft [m]	6.23
Deadweight tonnage [t]	7500

Table 7.1: Main data UT 745 (*Yno 227 - Mærsk Frontier 2020*)



Figure 7.1: UT 745 Platform Supply Vessel (*Yno 227 - Mærsk Frontier 2020*)

The ship is considered to impact one of the outer columns of the floater. With reference to Figure 6.7 the top diameter of this column is 13.4 m. The column model in LS-DYNA is created as a cylinder with constant cross section of 13.4 m in diameter, so the coned section is neglected. This is considered to have little influence on the result as this diameter is present from 9.5 m above to 4 m below MSL, and it is reasonable to assume that the impact will occur at this section.

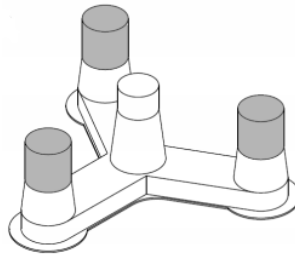


Figure 7.2: Columns exposed to ship impact (W. Yu, Müller, and Lemmer 2018)

The concrete material is expected to have minor deformations during a collision. Hence, rigid material model is assigned to the column. With reference to the design principles described earlier a strength design is assumed for OO Star Wind Floater. The column model is applied to both the different ship models, i.e the bulbous bow and ship-side. The mesh size chosen for the rigid column is element size of 0.1 m^2 .

The force-displacement curves for the ship is established by colliding the column into the ship model. Hence, the rigid column is free to translate in the impact direction but fixed in all the other five degrees of freedom. The contact between the two colliding structures is treated by the contact type "CONTACT_AUTOMATIC_SURFACE_TO_SURFACE" in LS-DYNA. Self contact within the structure is recommended to include for crash analyses, so the contact type "CONTACT_AUTOMATIC_SINGLE_SURFACE" is used.

Boundary prescribed motion is applied to the rigid column to achieve a constant impact velocity of $2 \frac{m}{s}$ throughout the analysis. The analyses are terminated based on user defined input and this varies for the two different models. For the bulbous bow the impact analyses are longer, meaning that the termination time is larger than for the ship-side model. One reason for this is that smaller deformations are expected for the ship side structure. Another reason is that the bow model is stable for larger crushing displacements. Hence, the termination time for the ship bow model is 4 seconds while it is 1.5 seconds for the side model.

7.1.1 Shiplside model

The supply vessel side model is displayed in Figure 7.3. The length, width and height of the segment is 15.6 m, 5.5 m and 7.6 m respectively. The ship model is based on structural drawings, with shell thickness varying from 7.5 mm to 25 mm. The thickness of the side girders in the bilge area is 9.5 mm, and the frame spacing is 650 mm. The material properties for the ship is a user defined steel material model. This material model implements a self-made material model, and LS-DYNA calls subroutines in order to define the material properties. One general remark is that failure of shell elements are allowed.

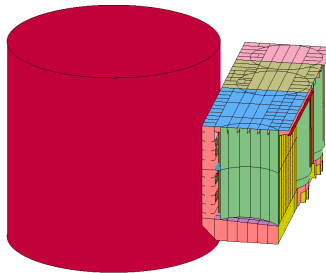


Figure 7.3: Shiplside model in LS-DYNA

The boundary conditions for the ship is defined at the longitudinal and transverse edges of the model's back-side. These edges are constrained in all rotational and translational degrees of freedom. The boundary conditions displayed in black in Figure 7.4 implies that the ship-side structure can be crushed by the column but not pushed away during the impact.

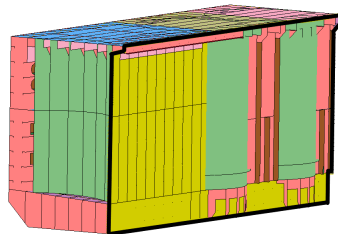


Figure 7.4: Boundary conditions prescribed node set shiplside

All the elements in the model are shell elements, and the formulation is Hughes-Liu elements. The theory behind this formulation is described in section 5.2.1.

7.1.2 Bow model

The ship bow model displayed in Figure 7.5 is based on structural drawings and the various decks, stringers and frames are modelled. In this work, the first 10 meters of the ship bow is considered. The plate thickness is 7 mm at the ship deck, and increases to 15 mm for the ring frames in the bulb. The hull thickness is 12 mm in the front part of the forecastle, while 12.5 mm in the bulb. There is 600 mm between the frames.

It is reasonable to establish two separate force-displacement curves for the bow, one for the bulb and one for the forecastle. This is achieved by translating the rigid column and isolating the crushing analysis for the different parts of the bow. Similarly as for the ship side impact, the column is prescribed rigid body velocity and the ship is fixed in all directions at the segment end.

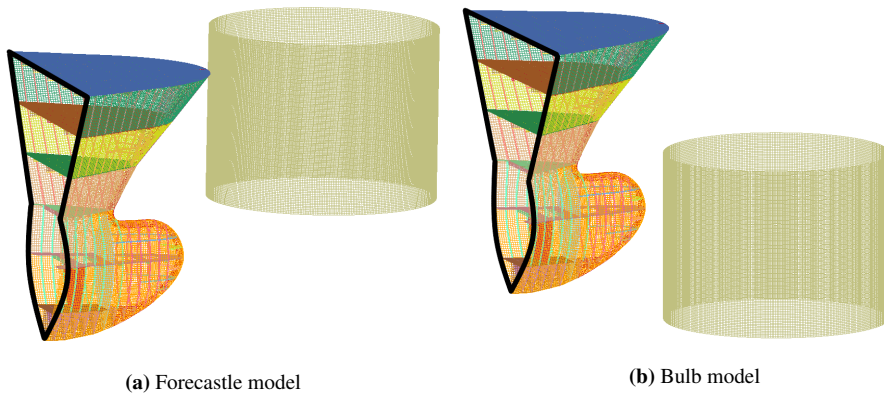


Figure 7.5: Ship bow model in LS-DYNA

The shell formulation used for the ship bow model is Belytschko-Tsay elements. One remark concerning the shell formulation used for the rigid column is that the same elements that are used for the ship model is used at the column. Hence, for the ship-side model Hughes-Liu formulation is used. It is expected that this will have little influence on the results, so consistency with provided models is considered.

7.2 Force-displacement curves

The force-displacement curves for the bulbous bow and ship side are needed for the global analyses in USFOS. Three individual force-displacement curves are extracted for the supply ship.

7.2.1 Shipside

The force-displacement curves for sideways impact of the concrete column is displayed in Figure 7.7. The crushing force is increasing steadily as the displacement increases, which indicates that the ship side is strong and dissipates a large amount of energy during deformation.

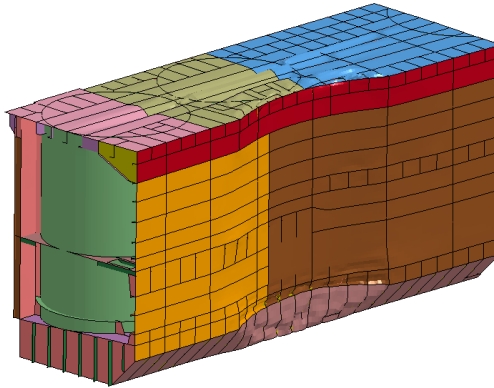


Figure 7.6: Crushing of ship side

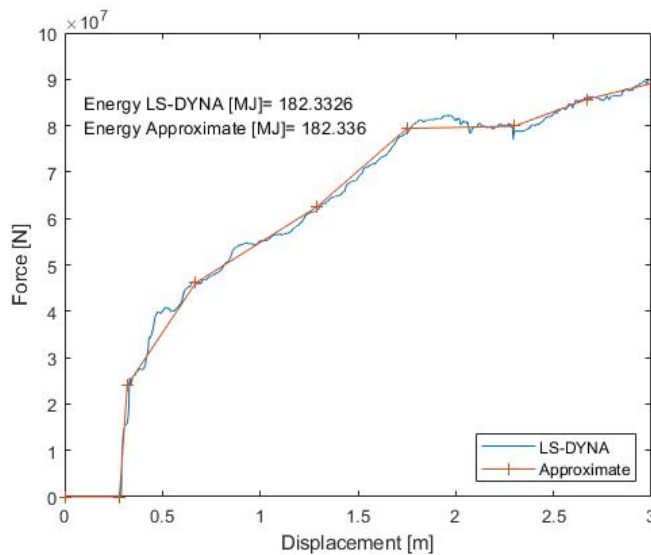


Figure 7.7: Force-displacement curve ship side

The approximate curve serves the purpose of being input to the global analyses in USFOS. Impact with the supply ship side is modelled by a single nonlinear spring, and the discrete

points in Figure 7.7 represents the force-displacement relationship of the supply vessel side. In order to represent the curve from LS-DYNA properly, similarity in the dissipated energy is considered important. The simplified curve is therefore made on the basis of this consideration, and the energy deviation between LS-DYNA and the approximate curve is small. The discrete points used as input in USFOS are summarized in Table 7.2

Force [MN]	Displacement [m]
0.0	0.0
0.0	0.28
24.0	0.32
46.1	0.67
62.5	1.29
79.4	1.75
79.9	2.3
85.7	2.67
89.1	3.0

Table 7.2: Force displacement curve for supply vessel side in USFOS

7.2.2 Bow

The force-displacement curves for the ship bow impacting the concrete column is separated into two contributions, one from the forecastle and one from the bulb section.

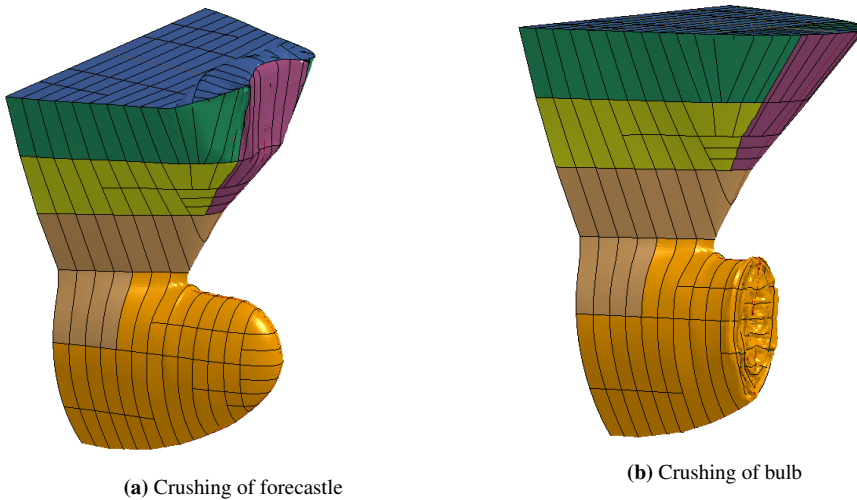


Figure 7.8: Crashing of bulbous bow LS-DYNA

Figure 7.9 displays the curves for the forecastle which is governed by bending and collapse of structural members. The force increases as the contact area grows. From the figure, the

first peak represent the initial contact with the uppermost deck, while the second peak represent the subsequent global buckling of the deck. The simplified curve follows the same principle as defined for the ship side, that is to have similarity in dissipated energy. The approximate model is not identifying the peaks very well, so modifications to include these may be reasonable to represent the crushing more accurately. However, after consultation with supervisor it was recommended to minimize lines with negative slopes as this can cause problems in USFOS. The discrete points used as input in USFOS are summarized in Table 7.3.

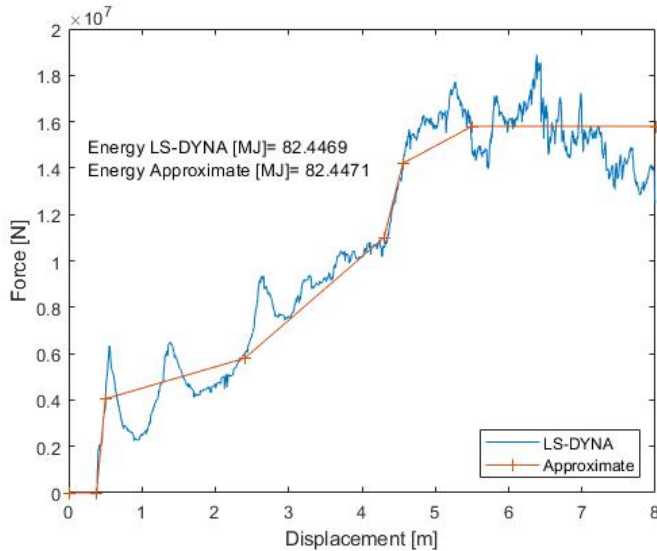


Figure 7.9: Force-displacement curve forecastle

Force [MN]	Displacement [m]
0.0	0.0
0.0	0.38
4.05	0.50
5.8	2.40
11.0	4.30
14.2	4.56
15.8	5.50
15.8	8.0

Table 7.3: Force displacement points forecastle

The crushing force of the bulb engages after 1.12 m crushing of the forecastle. The force attains a peak value at an early stage with maximum levels significantly higher than for the forecastle. The first peak represent the crushing of the front part of the bulb. Afterwards,

there are subsequent peaks which represent the crushing of transverse frames in the bulb. The discrete points used as input in USFOS are summarized in Table 7.4.

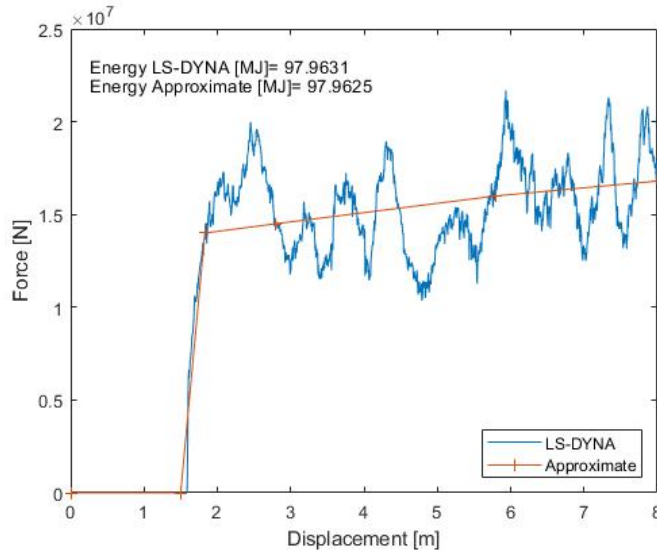


Figure 7.10: Force-Displacement curve Bulb

Force [MN]	Displacement [m]
0.0	0.0
0.0	1.50
14.0	1.83
14.5	2.8
16.0	5.8
16.8	8.0

Table 7.4: Force displacement points bulb

7.2.3 Recommended force-displacement relationship

Recommended practice for design against accidental loads by DNV GL display force-deformation relationship for standard supply vessels in the range from 6500 to 10 000 tonnes. These curves are displayed in Figure 7.11 where the curves for broad side, stern end and stern corner are based on impacts with a rigid cylinder. The curve for bow impact is based on collision with a rigid wall, and according to Amdahl, Solland, and Reitan (2017) the bow deformation curve for raked bow without bulb can be used for the fore-castle. The curves are applicable for collision with large diameter columns. Hence, they can be directly compared to the force-displacement curves established in LS-DYNA for the OO-Star Wind Floater column.

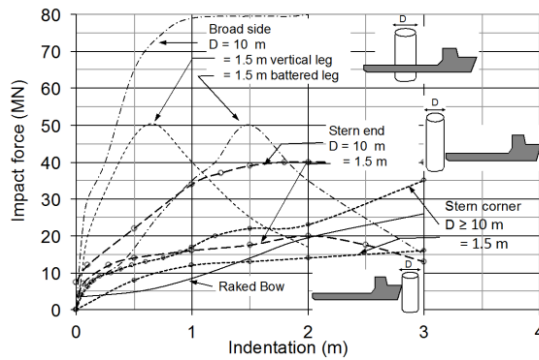


Figure 7.11: Force-Displacement curves DNV GL (Amdahl, Solland, and Reitan 2017)

The force-deformation curve for ship side is similar to the curve from DNV GL, i.e., both stabilize at an impact force of 80 MN. However, the curve established in LS-DYNA obtain this level after a little more indentation. The curve established for the forecastle can be compared to the curve for raked bow up to around one meter indentation. Despite that, the crushing characteristics after this indentation varies quite significantly, which makes it reasonable to not compare them directly. The reason for this is that bulbous bows differs from the standard vessel considered in NORSOK N-004.

The total crushing force versus deformation of the bow is plotted in Figure 7.12, and by comparing this curve to the raked bow it is clear that the crushing force is above the recommended raked bow curve. This is reasonable as the bulb has a much smaller cross-sectional area than the forecastle, so the intensity is higher. On the basis of this it is reasonable to assume that the bulb has the highest damage potential.

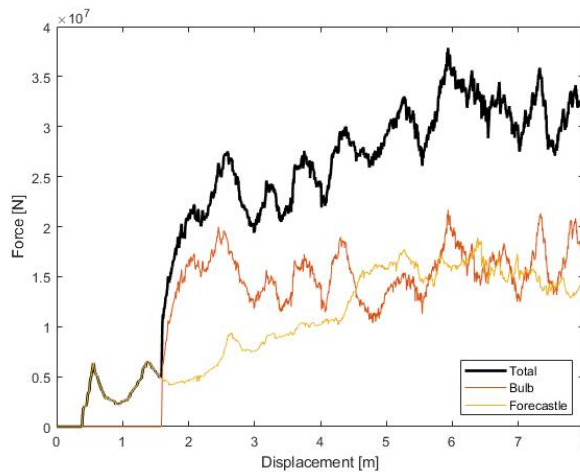


Figure 7.12: Force-displacement curve for supply vessel bow against rigid column

The isolated curves for the forecastle and bulb can be compared to a study in Martin Storheims doctoral thesis (Storheim 2015). The radius of the OO-Star Wind Floater column is 6.7 m, so the dark blue curves in Figure 7.13 is closest to the curves established in LS-DYNA.

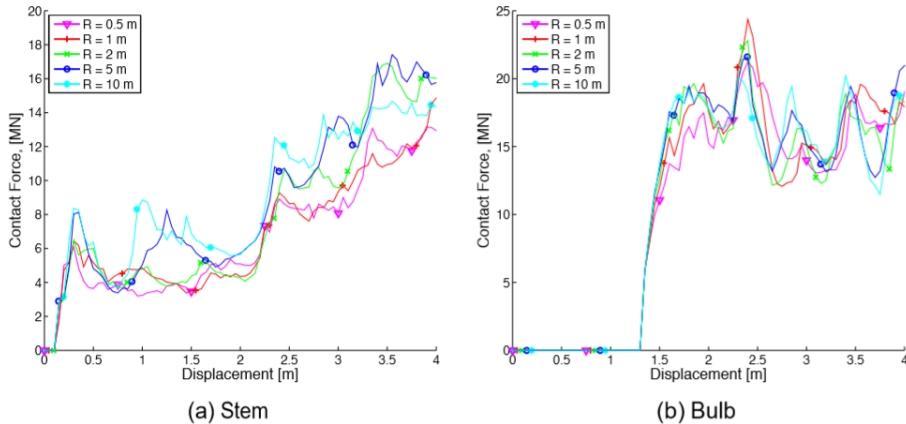


Figure 7.13: Force-displacement curve for supply vessel bow against rigid column with varying radius (Storheim 2015)

By comparing the curve for the forecastle with Storheim’s curve for the stem it is clear that the force levels obtained in LS-DYNA are lower. However, they both display similar shape, and a maximum level around 18 MJ is present in both curves. As to the lower force levels, this is not as expected. In reality it is assumed that the curve for the column with 6.7 m radius is in the range between the curves for R=5 m and R=10 m. Nevertheless, the variation is insignificant.

The bulb force in Figure 7.13 (b) is fairly independent of the column radius, and a steep increase up to 20 MN is present. Beyond this indentation, the force level oscillates around 17 MN. The reason for the bulb force being independent of the radius is that the global deformation mode is similar for the different column sizes. This is explained by the small cross-sectional area of the bulb. The same curve characteristics are present for the bulb curve established for the OO-Star Wind Floater column.

Comparison with the curves from Martin Storheim’s PhD verifies the force-displacement curves created for bow impact with OO-Star Wind Floater. Recommended curve from DNV GL verify the force-displacement curve for side impact. Based on this, all curves established in LS-DYNA is considered valid and ready to be used as input in USFOS.

7.3 Punching shear

Punching shear arise when concentrated loads are applied to a small area, and a typical failure takes place if the concrete column strength is smaller than the shear strength. The ductile fracture mode for reinforced concrete may change to brittle failure for punching shear failure, which can have catastrophic consequences for a floating structure (Zineddin and Krauthammer 2007). Penetration of the column wall can lead to subsequent flooding of compartments, which pose a significant threat to the safety of the floating structure (Sha and Amdahl 2019). Therefore, the collision resistance of the column walls should be evaluated so that progressive collapse is prevented.

In the event of a ship collision, the most critical scenario is in general impacts by the bulb. The small area with high localized forces pose a real threat for punching shear failure. In this thesis both side and bow impact are considered, so punching shear check is performed for both these impact scenarios.

Eurocode 2 - Design of concrete structures includes formulas for calculating the punching shear stress for reinforced concrete slabs. According to this standard, the shear stress, ν_{Ed} , at the loading perimeter should not exceed the shear capacity, $\nu_{Rd,max}$.

$$\nu_{Ed} \leq \nu_{Rd,max} \quad (7.1)$$

where the shear stress is calculated by

$$\nu_{Ed} = \beta \frac{V_{Ed}}{u_0 d} \quad (7.2)$$

In Equation 7.2, $\beta=1.15$ is a factor accounting for eccentricity, V_{Ed} is the shear force, u_0 is the length of the loading perimeter and d is the effective depth of the concrete column wall (ibid.). The expression for shear capacity may vary in different countries, but the recommended value is $0.4\nu f_{cd}$. Inserting the recommended value for ν give the following equation:

$$\nu_{Rd,max} = 0.4 \times 0.6 \left[1 - \frac{f_{ck}}{250} \right] f_{cd} \quad (7.3)$$

where f_{cd} and f_{ck} are the design and characteristic cylinder compressive strength. Concrete specifications for OO-Star Wind Floater is not public, so reference is made to Sha and Amdahl (ibid.) where $f_{cd}=60\text{MPa}$ and $f_{ck}=50\text{MPa}$. These properties are used for the pontoon walls for a floating bridge concept, so they are considered appropriate to use for the FOWT.

In addition to calculating the stress at the loading perimeter, the stress also needs to be checked at the basic control perimeter. According to *Eurocode 2* (2004) the basic control perimeter u_1 is taken at a distance of $2.0d$ from the loaded area.

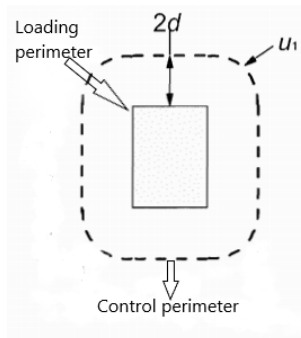


Figure 7.14: Basic control perimeter around loaded area *Eurocode 2* (2004)

$$\nu_{Ed} \leq \nu_{Rd,c} \tag{7.4}$$

$$\beta \frac{V_{Ed}}{u_1 d} \leq C_{Rd,c} k (100 \rho_1 f_{ck})^{1/3} \tag{7.5}$$

where $\nu_{Rd,c}$ is the capacity at the basic perimeter. $C_{Rd,c}=0.12$ and $k = 1 + \sqrt{\frac{0.2}{d}} \leq 2$ are recommended size coefficients, and $\rho_1 \leq 0.02$ is recommended reinforcement ratio. Equation 7.1 and 7.5 are used as punching shear checks, where the shear force included in these equations are taken as the impact load from the numerical analyses in LS-DYNA. From the analyses the impact force is time-dependent. Hence, the numerical shear forces also vary with time, giving a dynamic punching shear check. Specifications for the concrete is not publicly available, so for the checks in this thesis the concrete thickness varies. Hence, the reinforcement ratio is chosen as the maximum value, i.e $\rho_1 = 0.02$.

For both the ship side and bulb impacts a $1 \cdot 1 \text{m}^2$ area and $3 \cdot 2 \text{m}^2$ area is used for calculating the shear force. The control perimeter length can then be determined based on the thickness of the concrete.

Thickness d [m]	u_0 [m]	u_1 [m]
0.3	4	8.8
0.4	4	10.4
0.5	4	12

Table 7.5: Loading and control perimeter 1 m^2

Thickness d [m]	u_0 [m]	u_1 [m]
0.3	10	14.8
0.4	10	16.4
0.5	10	18

Table 7.6: Loading and control perimeter 6 m^2

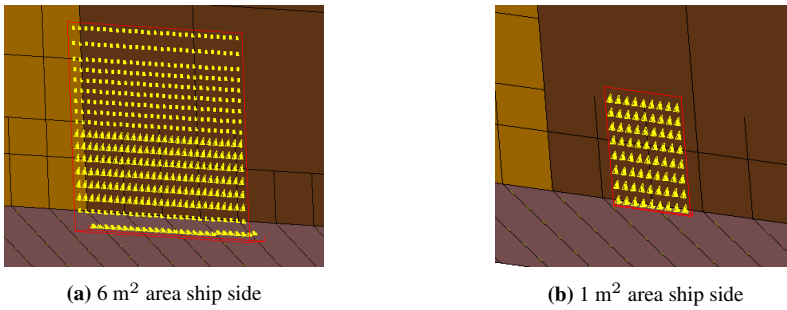


Figure 7.15: Nodal points used for force extraction ship side

The design and characteristic compressive strength of the concrete give a shear capacity of 11.5 MPa at the loading perimeter. For all the different scenarios considered, the maximum shear stress at this perimeter is much lower than the capacity. However, at the control perimeter the shear stress and the capacity are in the same region. Main focus from the punching shear check is therefore put at the control perimeter. Punching shear checks for a column thickness of 0.4 m are displayed in Figure 7.16 and 7.17, while the rest of the results can be found in Appendix A.

The shear stress history at the loading perimeter is represented by the blue curves in Figure 7.16 and 7.17. Punching shear failure at this perimeter is no risk for any of the design thicknesses. On the other hand, the capacity at the control perimeter is 0.95 MPa, and by evaluating the orange curves a general risk for punching shear is present. Figure 7.16b display the shear stress history for a 6 m^2 contact area at the ship side, and at the control perimeter, the shear stress becomes larger than the capacity between 0.16 and 0.35 seconds. In this region the concrete column wall fails with a thickness of 0.4 m.

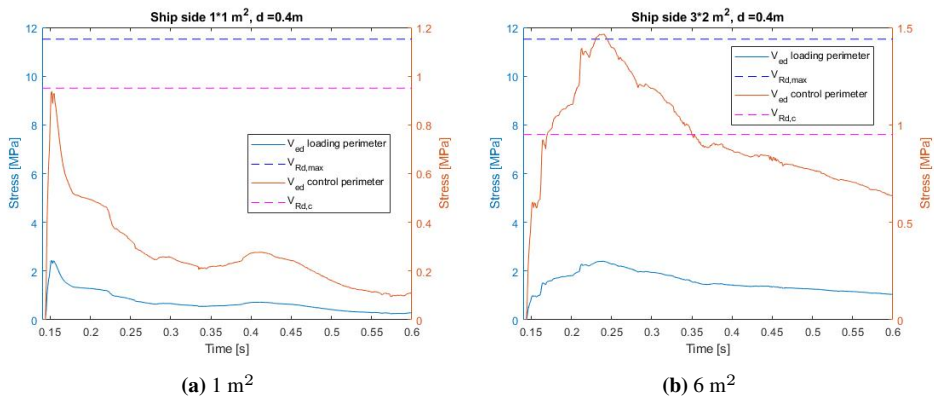


Figure 7.16: Punching shear design ship side

The shear stress histories for different contact areas for bulbous bow impact are given in Figure 7.17. The shear stress at the control perimeter for a contact area of 6 m^2 is exceed-

ing the capacity for a short period of time at the beginning. At this stage, the contact area is small and loading short-lived, so it might not lead to punching failure of the concrete wall. However, for the 1 m² contact area the shear stress intensity is higher and acts for a longer period of time over the capacity, which make punching shear failure possible.

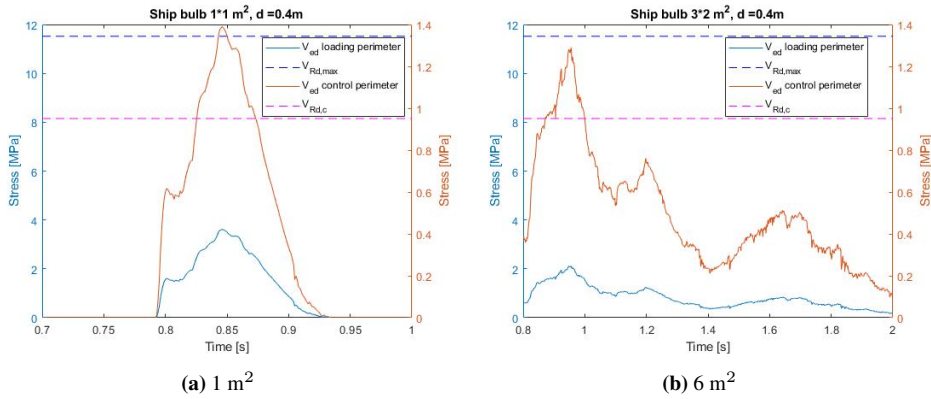


Figure 7.17: Punching shear design ship bulb

Hong, Amdahl, and G. Wang (2009) calculated pressure-contact area combinations for a 7500 ton supply vessel bulb. The relationship between the pressure, P [MPa], and contact area, A [m²], could be represented by:

$$P = 7A^{-0.7} \tag{7.6}$$

Inserting for areas of one m² and six m² give pressures of 7 MPa and 2 MPa, respectively. Compared to the blue curves in Figure 7.17 it correspond well for the largest area. For the smallest area the deviation is larger, and one of the reasons might be related to the difference in impact forces for a rigid wall and rigid column. Another reason might be related to the area definition for force extraction in LS-DYNA.

Generally, the shear capacity at the loading perimeter is sufficient for all the different collision loads. However, at the control perimeter the shear stress is close to or exceeds the capacity, causing a possibility for punching failure. This failure is critical for the structure, and flooding of compartments is the result. According to DNVGL-ST-0119 (2018) the global structural integrity shall maintain after flooding, and this standard states that thorough documentation is needed for collision on floating structures.

The risk of punching shear failure is present for a thickness of 0.4 m or less. Based on parameters used for floating bridges, it is reasonable to assume that the thickness of the concrete columns on OO-Star Wind Floater is greater than 0.4 m. Additionally, the other parameters used in the calculations are based on other studies, and more accurate result for the floater is achieved by obtaining the correct data. All in all, performing a punching shear check in the preliminary design phase can be valuable in order to determine some of the main parameters of the structure.

Global analysis in USFOS

Impacts from unintended collisions are accidental loads that are important to consider for floating support structures. In this accidental limit state, nonlinear effects are present, and USFOS is a computer program suitable for evaluating global behavior. In this chapter, global collision analyses for parked and operating FOWT are considered. Broadside and bow impact for a supply vessel are evaluated, and multiple different collision scenarios are investigated. The main parameters for the analyses are summarized in Table 8.1

Shipside Impact		Ship Bow Impact	
Parameter	Value	Parameter	Value
Weight [tonnes]	7500	Weight [tonnes]	7500
Velocity [m/s]	2	Velocity [m/s]	3
Time for initialization of impact [s]	100	Time for initialization of impact [s]	100
Hydrodynamic added mass [%]	40	Hydrodynamic added mass [%]	10

Table 8.1: Parameters ship impacts in USFOS

OO-Star Wind Floater has three outer columns that all are exposed to ship impacts. Generally, collision damage is somewhat dependent on the position of the impact (G. Wang, Arita, and Liu 2000). For that matter, collision scenarios on two different columns are considered. In addition to this, three different directions of impact are analyzed for each of the columns. Considering that all analyses are performed for both parked and operating turbines, 24 impact scenarios are investigated, 12 for PSV bow impact and 12 for PSV side impact. The directions of impact are in global x- and y-direction and diagonally in xy-direction. Figure 8.1 display the global reference system and column specification.

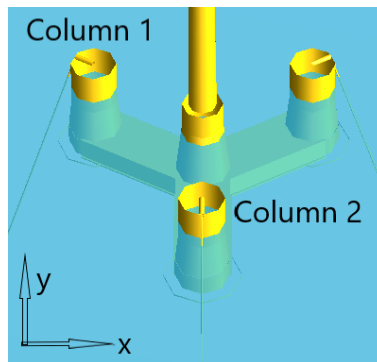


Figure 8.1: Collision scenarios description

The most severe condition for ship-ship impact is generally accepted to be when the struck ship is at standstill (Kitamura 2002). The same analogy is used for the ship-FOWT impacts, so the floating structure is at rest at the time of impact. In operational condition the structure is stationary after around 100 seconds, which is why the collision is initiated at this time instant.

8.1 Model verification

Prior to the collision analyses in USFOS, the ship collision model described in Section 6.5 needs verification. The force-displacement curves for the bulbous bow and ship side established in LS-DYNA are given as input for the nonlinear springs in USFOS. It is essential to verify that the output curves from USFOS coincide with the input curves specified.

The models for the ship bow and side are described in Chapter 7, and implementing these into USFOS are done by nonlinear springs. The positioning of the spring system is based on the structural properties of the UT745 Platform Supply Vessel. In Section 6.5 the spring system used for bulbous bow is described, where one spring is located in the center of the bulb and one at the center of the forecastle. The distance between these two centers is 8.3 m. Considering that the draft of the PSV is 6.23 m, the location of the bulb springs is 1.5 m below MSL. Impacts by ship side are, on the other hand, represented by one single nonlinear spring. The height from the keel to the main deck is 7.6 m. The spring is assumed to be located in the center, i.e., 2.4 m below MSL.

Force-displacement curves for bulb and forecastle

The input curves for the forecastle and bulb are compared to the output curves from USFOS in Figure 8.2. From the figures, it is clear that the curves coincide, and that unloading follows the same path as the loading. This property is in accordance with the hyperelastic material behavior specified for the nonlinear springs.

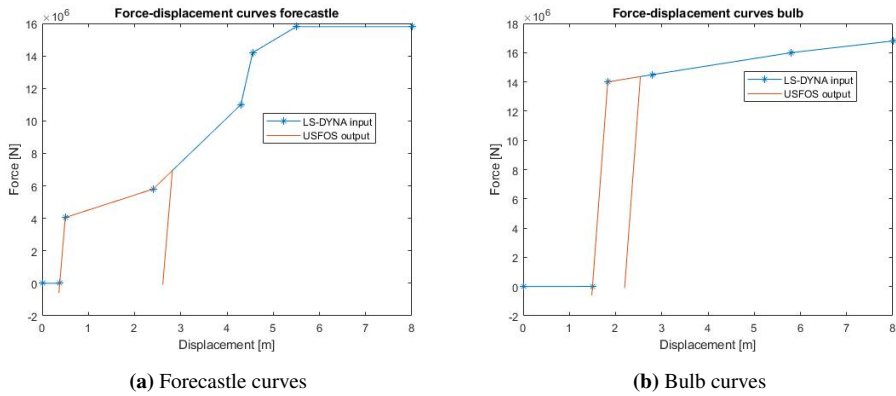


Figure 8.2: Comparison force-displacement curves forecastle and bulb

The bulb force engages after 1.12 m crushing of the forecastle. In USFOS, this is accounted for by modifying the linear spring for the bulb. Originally, the stiffness is $1E+08$ N/m in compression. Adjustment is made so that the bulb spring is activated after compression of 1.12 m is present. Figure 8.3 display the property for the linear spring in the axial direction.

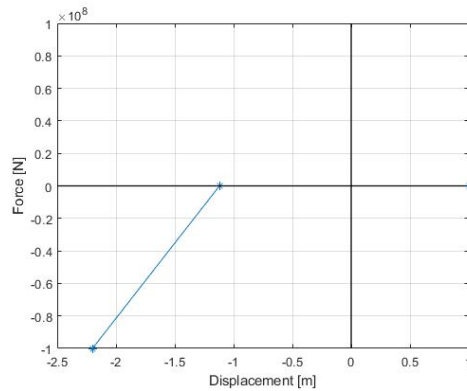


Figure 8.3: Linear spring bulb

All the other linear springs are activated at the moment compression occurs.

Force-displacement curves for side impact

The output curve from the analysis in USFOS is compared to the input curve from LS-DYNA in Figure 8.4.

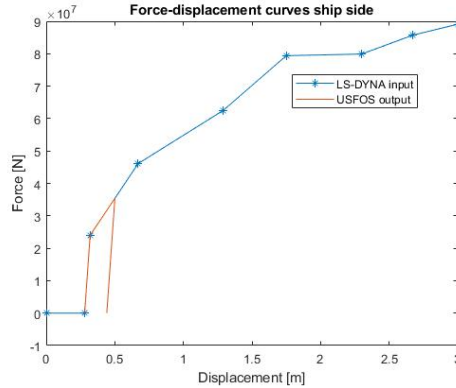


Figure 8.4: Comparison force-displacement curves ship side

Similarly as for the bow, the output curve and the input curve coincide for broadside impact. This result verify that the collision system represents the ship correctly. Chapter 6 includes verification executed for the turbine blades, tower and the floating structure, and by including the verification of the collision system, the total FOWT model is considered sufficiently accurate. Based on this, the model is prepared for global response analyses.

8.2 Collision analyses for wind turbine in parked condition

During weather conditions where the wind speed is below the cut-in speed or the wind turbine is under maintenance, the FOWT is in parked condition. Stationary turbine blades represent this. Hence, structural performance of the FOWT in parked condition subjected to ship impacts is investigated by having stationary blades and no wind loads. Regarding the latter assumption, this is somewhat questionable as forces from the wind in general always are present. However, these loads are not included. Multiple different responses of the FOWT are investigated in parked condition.

8.2.1 Moment in tower

The wind turbine tower is an unstiffened cylindrical shell and shall be designed against buckling. Buckling of these members are in general more violent than it is for plates and columns, and initial imperfections cause the buckling load to be significantly lower than for perfect shells.

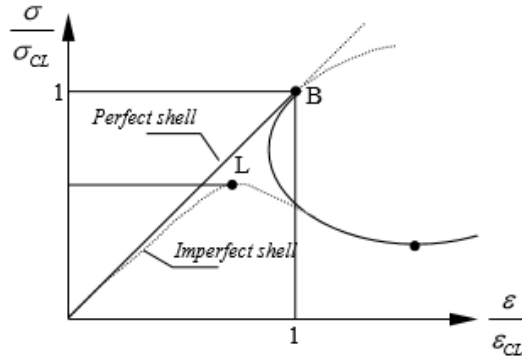


Figure 8.5: Equilibrium path for perfect and imperfect shells according to Amdahl (2010)

According to Amdahl (2010), an imperfection amplitude of 1/10 of the wall thickness reduces the theoretical buckling load by 40%. Therefore, the inherent sensitivity to imperfections for cylindrical shells cause modifications to the theoretical load by an empirical reduction factor. This factor is often denoted a knock-down factor.

Tubular members subjected to axial compression can fail by material yielding or local buckling, and the diameter to thickness ratio influences the failure mechanism (Amdahl 2013). For members with a low D/t ratio, the design is in general based on material yielding, while for larger ratios, the elastic buckling strength decreases. In the event of an impact with OO-Star Wind Floater, the turbine tower is exposed to large forces and moments. The lowest segment, i.e., the section connected to the floater, suffers the most significant risk for shell buckling. Properties for this section are given in Table 8.2.

Diameter	Thickness	D/t	Young's modulus	Yield strength
8.30 [m]	0.038 [m]	218.42	210E+03 [MPa]	355 [MPa]

Table 8.2: Properties lower segment of wind turbine tower

According to *DNV-RP-C202* (2013) the elastic buckling strength for unstiffened cylindrical shells is

$$\sigma_E = C \frac{\pi^2 E}{12(1-\nu^2)} \left(\frac{t}{l} \right)^2 \quad (8.1)$$

where the reduced buckling coefficient can be determined by

$$C = \psi \sqrt{1 + \left(\frac{\rho \xi}{\psi} \right)^2} \quad (8.2)$$

This formula is applicable for combined load cases. The bending moment is considered to be most critical, but the axial force at the tower intersection is also included. For these load cases $\psi = 1$ and $\xi = 0.707 Z_l$, where Z_l is the curvature parameter given by

$$Z_l = \frac{l^2}{rt} \sqrt{1 - \nu^2} \quad (8.3)$$

The imperfection sensitivity introduces a knock-down factor ρ which varies for axial compression and bending. *DNV-RP-C202* (2013) uses:

$$\rho = \begin{cases} \frac{0.5}{\sqrt{1 + \frac{r/t}{150}}} & \text{- Axial compression} \\ \frac{0.5}{\sqrt{1 + \frac{r/t}{300}}} & \text{- Bending} \end{cases} \quad (8.4)$$

Calculating the different parameters based on the tower segments' geometrical properties results in elastic strength of 442 MPa and 500 MPa for axial and bending stress, respectively.

The knock-down factor for shape imperfections is essential both in the elastic and elastoplastic range. Modifying the elastic critical stress for plasticity is achieved by calculating the characteristic buckling strength. The critical stress is defined by

$$\sigma_{eq,cr} = \frac{1}{\sqrt{1 + \bar{\lambda}_{eq}^4}} \sigma_Y \quad (8.5)$$

where the slenderness parameter $\bar{\lambda}_{eq}^2$ is given as

$$\bar{\lambda}_{eq}^2 = \frac{\sigma_Y}{\sigma_{eqE}} = \frac{\sigma_Y}{\sigma_{eq}} \left(\frac{\sigma_x}{\sigma_{xE}} + \frac{\sigma_b}{\sigma_{bE}} \right) \quad (8.6)$$

$$\sigma_{eq} = \sqrt{(\sigma_x + \sigma_b)^2} \quad (8.7)$$

The utilization factor is a measure of the ratio between the equivalent stress and the critical equivalent stress. This factor should be smaller than one in order to have an adequate design with respect to the elastoplastic buckling of the tower.

$$\eta = \frac{\sigma_{eq}}{\sigma_{eq,cr}} \leq 1 \quad (8.8)$$

Bending stress, σ_b , and axial stress, σ_x , at the tower intersection are collected for all the different collision scenarios, and the utilization factors are computed. The results are summarized in Tables 8.3, 8.4, 8.5 and 8.6.

Ship Bow Impact Parked Condition			
Column 1			
Global direction	σ_x [MPa]	σ_b [MPa]	Utilization factor η
X	13.9	152	0.57
Y	13.9	155	0.59
XY	13.9	127	0.49

Table 8.3: Stresses in tower for ship bow impact in parked condition on Column 1

Ship Side Impact Parked Condition			
Column 1			
Global direction	σ_x [MPa]	σ_b [MPa]	Utilization factor η
X	13.9	166	0.62
Y	13.9	152	0.58
XY	13.9	118	0.48

Table 8.4: Stresses in tower for ship side impact in parked condition on Column 1

Ship Bow Impact Parked Condition			
Column 2			
Global direction	σ_x [MPa]	σ_b [MPa]	Utilization factor η
X	13.9	166	0.54
Y	13.9	169	0.63
XY	13.9	109	0.43

Table 8.5: Stresses in tower for ship bow impact in parked condition on Column 2

Ship Side Impact Parked Condition			
Column 2			
Global direction	σ_x [MPa]	σ_b [MPa]	Utilization factor η
X	13.9	138	0.53
Y	13.9	184	0.69
XY	13.9	112	0.44

Table 8.6: Stresses in tower for ship side impact in parked condition on Column 2

In parked condition the utilization factors are well below the limit, which indicates that the tower design is adequate with respect to elasto-plastic buckling. The collision scenarios that are worst in terms of utilization factor are going to be investigated further in parked condition. These scenarios are:

- Side impact
 - Column 1- Global x-direction
 - Column 1- Global xy-direction
 - Column 2- Global y-direction
- Bow impact
 - Column 1- Global x-direction
 - Column 1- Global xy-direction
 - Column 2- Global y-direction

8.2.2 Acceleration of nacelle

In Chapter 4 different consequences of ship collision are presented, and acceleration of the nacelle is a threat to electricity production. Therefore, monitoring this response is important, and exceeding the proposed range of 0.2-0.3 g can have severe economic consequences.

Figure 8.6 display the nacelle accelerations for three different collision scenarios for PSV side impact. The collision is initiated after 100 seconds, and from the figure, it is clear that the electrical equipment is endangered for all scenarios. However, impacts in x-direction on column one and y-direction on column two are more violent.

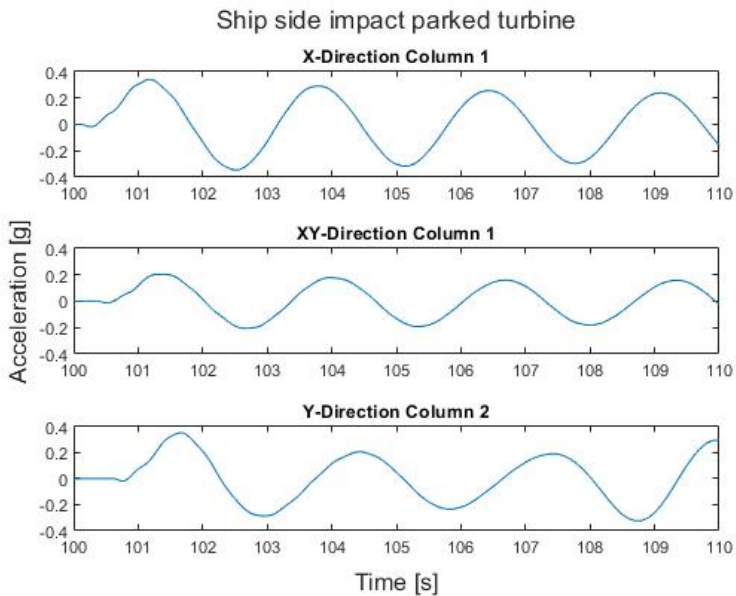


Figure 8.6: Acceleration of nacelle side impact parked condition

Impact by bulbous bow is less severe than impact by ship side concerning accelerations of the nacelle, and the results are presented in Figure 8.7. In a similar manner as broadside impact, the critical directions are parallel to the rotor plane on column one and normal to the rotor plane on column two. The maximum levels are less critical for bow impact, so the electrical equipment might withstand these collision scenarios.

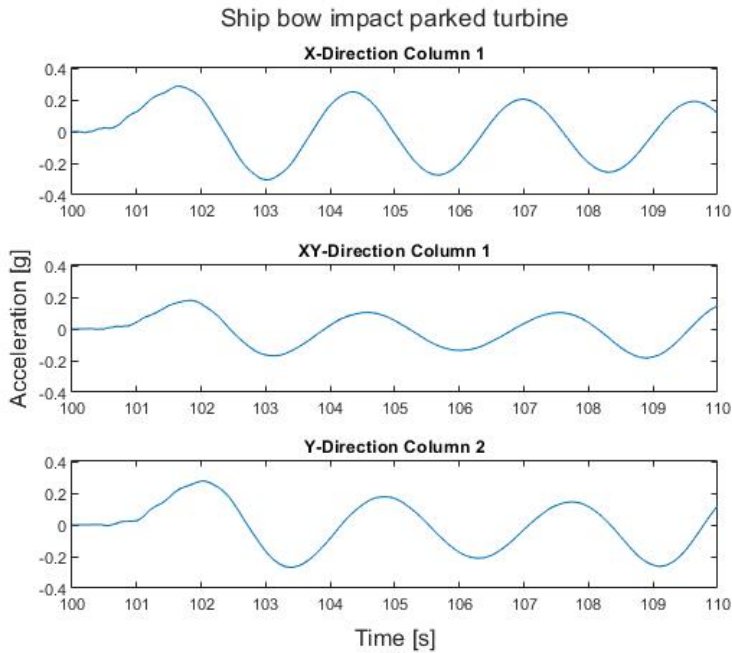


Figure 8.7: Acceleration of nacelle bow impact parked condition

8.2.3 Kinetic energy

The collision energy is determined based on the ship mass and impact velocity. In the event of an collision with the FOWT in parked condition, the impact energy can be simplified to the expression (Veritas-NI-572 2019):

$$E_c = 0.5 (m_s + a_s) v_s^2 \quad (8.9)$$

Inserting the properties given in Table 8.1 give collision energies of 21 MJ and 37 MJ for side and bow, respectively. Parts of the kinetic energy remain kinetic, while the rest is dissipated as strain energy by structural deformations. Shiplside impact on column two normal to the rotor plane is considered, and the amount of energy dissipated by the ship can be determined based on the force-displacement curve.

Figure 8.9a display the kinetic energy for the FOWT model in USFOS. After 100 seconds, the peak corresponds well to the calculated impact energy of 21 MJ. Before this point, peaks in kinetic energy are present, and a large peak occurs after a few seconds. The reason for this is the initialization of the floating structure, where gravity and buoyancy forces are applied. The equilibrium position is reached quickly as the energy decreases rapidly. Figure 8.9b display the output force-displacement curve for the ship side.

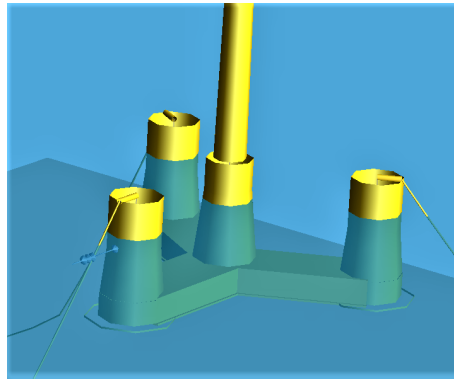


Figure 8.8: Side impact on column 2

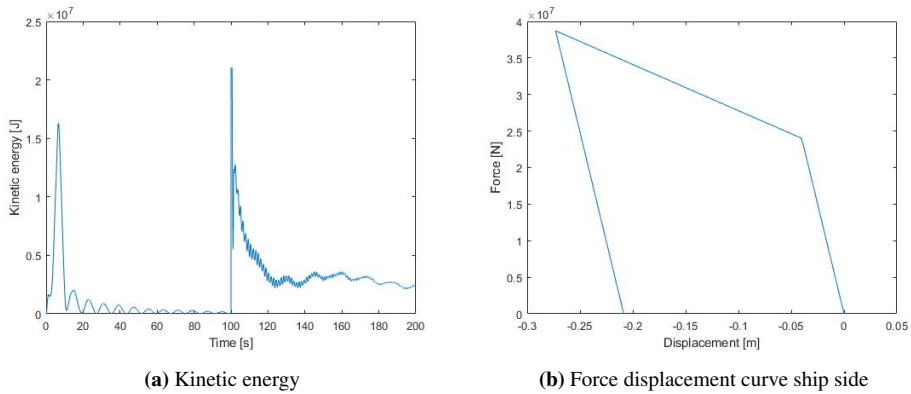


Figure 8.9: Kinetic energy and force displacement curves ship side collision

Trapezoidal integration of the force-displacement curve gives a total of 6.5 MJ that is dissipated by structural deformations in the ship. Generally, a simplified expression for determining the strain energy is:

$$E_s = \frac{1}{2} (m_s + a_s) v_s^2 \frac{1}{1 + \frac{m_s}{m_i}} \tag{8.10}$$

Inserting for side impact, the strain energy is 16.7 MJ. This means that 16.7 MJ of the total collision energy is dissipated by structural deformation in the ship and FOWT. Considering the energy dissipated by the ship, a total of 10.2 MJ shall be dissipated by the FOWT. The remainder, i.e., 4.3 MJ remains kinetic after impact.

8.2.4 Distance between blade tip and tower

Maximum blade tip deflection is an important design parameter, and the blades must be kept at a safe distance from the turbine tower (Brøndsted and P.L Nijssen 2013). For that matter, the blades often have a prebend, the rotor has a precone angle and the shaft is tilted. All these effects increase the tower clearance. Monitoring the clearance during a collision is reasonable as the consequence of an impact between the turbine tower and the blade is severe, causing downtime and economic losses.

The tower clearance for the reference turbine is 18.3 m without loads. The model in US-FOS has a clearance of 5.7 m, as precone is the only property that is considered. The relative displacement between the tower and the blade tip during broadside and bow collision in parked condition are displayed in Figure 8.10. The worst impact scenario is considered, i.e., when the impact occurs normal to the rotor plane on column two.

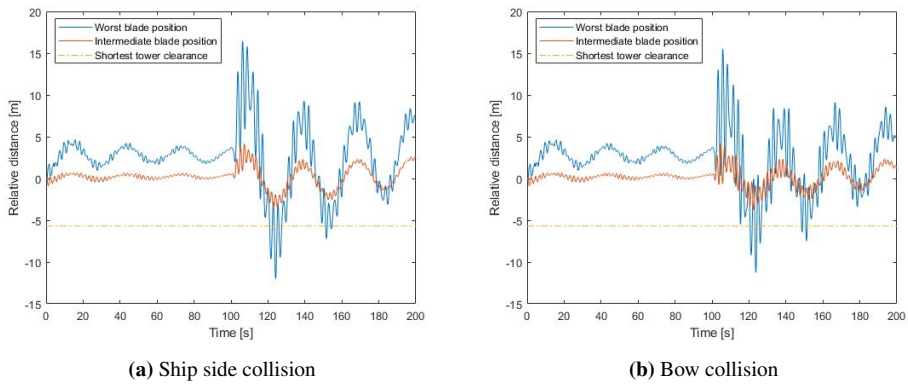


Figure 8.10: Relative distance tower and blade tip in parked condition

For each of the figures, the relative displacement is computed for two different blades. The layout describing the curves is presented in Figure 8.11.

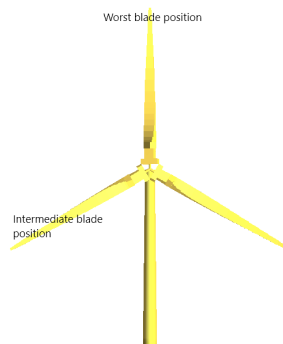


Figure 8.11: Layout description for blades in parked condition

The worst position for the blades with respect to the relative displacement exceeds the shortest tower clearance after around 120 seconds for both impact scenarios. Regarding tower impact, this will occur if the blade is parallel to the tower. By considering the results, it is reasonable to assume that the blade can hit the tower during a collision. However, the ship impact also induce tower displacement, and general bending of the tower will influence the relative displacement. Modeling one of the turbine blades parallel to the tower is proposed to increase the accuracy.

8.2.5 Mooringline forces

Evaluating the mooring line forces is necessary to determine if they can withstand the collision loads. Prior to the collision, the forces are equal to the pretension in the lines. In operational condition, some of the lines will have increased load due to the global loading of the FOWT. Based on this, the mooring line forces are only evaluated in operational condition as this is considered more critical.

8.3 Collision analyses for wind turbine in operating condition

Ship collisions are a risk that is present also for operating wind turbines. This is represented by rotating turbine blades and wind forces acting on the blades. In section 6.1 the procedure for calculating the drag and lift forces on the turbine blade is highlighted. In operating condition these forces are applied as nodal forces on the blade segments. Although the wind forces are based on the relative velocity, a factor of 0.5 is applied to all forces. The reason is that the forces influence the global response of the FOWT too significantly, and after consultation with the supervisor a reduction of 50 % is recommended. Therefore, the total applied forces are reduced from $2.2\text{E}+06$ N to $1.1\text{E}+06$ N.

Similarly as to the parked FOWT, multiple different responses are investigated with respect to collision with the operating turbine. The basis for the collision scenarios are the same, and a description of the reference system and column specification is reproduced in Figure 8.12.

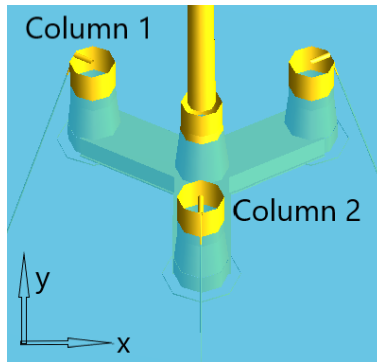


Figure 8.12: Collision scenarios description

8.3.1 Moment in tower

Buckling considerations are based on the same theory and calculations performed for parked turbine, so reference is made to Section 8.2.1. Utilization factors for all collision scenarios are calculated and summarized in the following tables.

Ship Bow Impact Operating Condition			
Column 1			
Global direction	σ_x [MPa]	σ_b [MPa]	Utilization factor η
X	13.9	146	0.55
Y	13.9	226	0.83
XY	13.9	179	0.67

Table 8.7: Stresses in tower for ship bow impact in operating condition on Column 1

Ship Side Impact Operating Condition			
Column 1			
Global direction	σ_x [MPa]	σ_b [MPa]	Utilization factor η
X	13.9	175	0.65
Y	13.9	224	0.82
XY	13.9	195	0.72

Table 8.8: Stresses in tower for ship side impact in operating condition on Column 1

Ship Bow Impact Operating Condition			
Column 2			
Global direction	σ_x [MPa]	σ_b [MPa]	Utilization factor η
X	13.9	138	0.53
Y	13.9	234	0.86
XY	13.9	179	0.67

Table 8.9: Stresses in tower for ship bow impact in operating condition on Column 2

Ship Side Impact Operating Condition			
Column 2			
Global direction	σ_x [MPa]	σ_b [MPa]	Utilization factor η
X	13.9	149	0.57
Y	13.9	240	0.88
XY	13.9	216	0.80

Table 8.10: Stresses in tower for ship side impact in operating condition on Column 2

Generally, the consequences in operational condition are worse than for parked condition. The utilization factors are higher, and some scenarios are close to the limit, meaning that buckling of the tower is an actual danger. However, notice should be made to the calculations as conservative factors are used to determine the critical stress. With these factors applied, all utilization factors below one are considered adequate.

Broadside and bow collision normal to the rotor plane on column 2 are the most critical scenarios. Shell elements can be generated in the lower part of the tower in order to investigate possible local buckling in USFOS.

In the lower part of the tower, a five-meter beam segment is replaced by shell elements. The diameter of the tower is 8.3 m and the shell element substructure consists of 25 elements in the longitudinal direction and 130 elements in the circumferential direction. This gives a quadrilateral mesh size of 0.04 m².

The effect of local imperfections on shell elements are substantial. Including this in USFOS is therefore important. According to *DNVGL-OS-C401* (2015), the maximum imper-

fection tolerance for circular cylindrical shell is given by:

$$\delta = \frac{0.01g}{1 + \frac{g}{r}} \quad (8.11)$$

where g denote the length of template or rod and r is the radius of the tower. An eigenvalue analysis on the shell segment is used to determine the imperfection shape. The buckling mode creates a total number of 8 half-waves in the circumferential direction. Reference is made to Figure 8.13. The length of the rod is determined based on the tower's perimeter divided on the number of half-waves. Inserting into Equation 8.11 gives maximum allowable imperfection tolerance of 18 mm. Implementation of imperfection in USFOS is done by using the command BUCKMODE, which scales a specified eigenmode by a factor. The nodal points are then updated so that the shape of the eigenmode is represented. The first eigenmode is chosen as the imperfection shape, and in accordance with the code, a scale factor of 0.018 is applied.

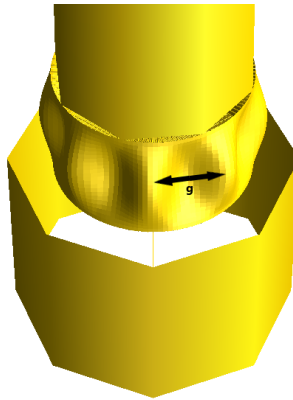


Figure 8.13: Eigenmode shell substructure

Ship impact by side is evaluated with shell substructure, and the specified speed according to codes is used. Local buckling of the tower structure does not occur for this scenario, so buckling is triggered by increasing the impact speed. For broadside impact, elastoplastic buckling occurs for a ship speed of 5 m/s. Figure 8.14 display the plastic utilization at the tower intersection prior to the collapse. The impact scenario causes local buckling, and the consequence is that the tower falls in the direction of the ship. With reference to Chapter 4, the preferred response is that the tower falls away from the ship. Hence, buckling of the tower is catastrophic, and injuries or fatalities are possible consequences.

It should be mentioned that these results are based on a scale factor of 0.018 on the first eigenmode. Increasing the imperfection will yield lower capacities, which means that the tower will buckle for lower impact speeds.

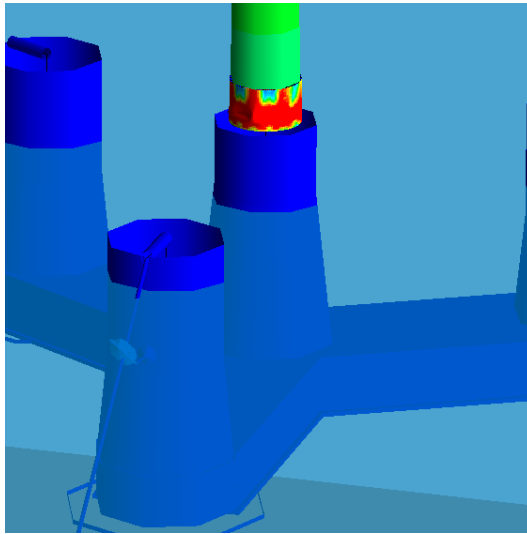


Figure 8.14: Local buckling of tower

In a similar manner as for parked condition, the worst collision scenarios with respect to stresses in tower are used for further response investigations. For the operating turbine these collision scenarios are:

- Side impact
 - Column 1- Global y-direction
 - Column 2- Global xy-direction
 - Column 2- Global y-direction

- Bow impact
 - Column 1- Global y-direction
 - Column 2- Global xy-direction
 - Column 2- Global y-direction

8.3.2 Acceleration of the nacelle

Accelerations of the nacelle during a collision in operating condition should not exceed 0.2-0.3g. Figure 8.15 display the nacelle accelerations for three different scenarios for PSV side impact. The collision is initiated after 100 seconds, and from the figure, it is clear that the electrical equipment is endangered. The worst scenario is collision normal to the rotor plane on column two.

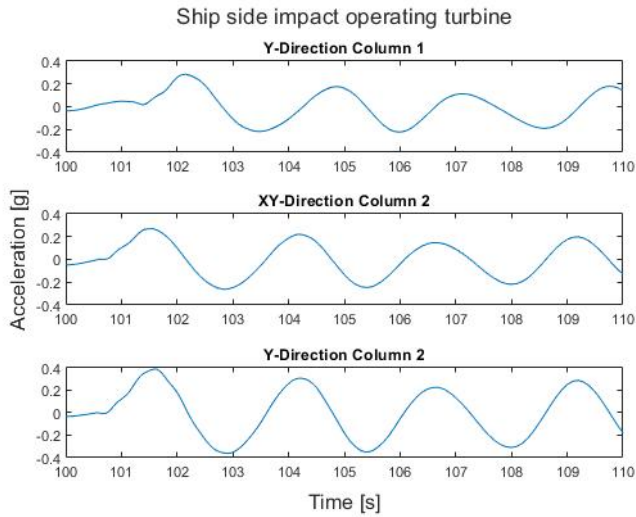


Figure 8.15: Acceleration of nacelle side impact operating condition

Collision by bow is less severe than collision by ship side, and the results are presented in Figure 8.16. The critical range is exceeded only for impact in global y-direction on column two.

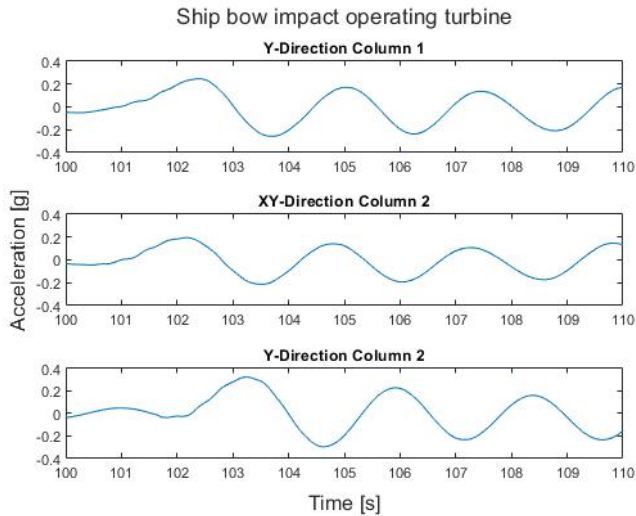


Figure 8.16: Acceleration of nacelle bow impact operating condition

All in all, ship impact poses a real threat to the wind turbine's electrical equipment. The worst consequences are occurring for side impact.

8.3.3 Distance between blade tip and tower

The tower clearance is 5.7 m without loading in USFOS. In operational condition the wind loads cause deflection of the turbine blades. Hence, the tower clearance decreases. The magnitude of the deflection is interesting to evaluate, and this is determined by keeping the tower top fixed in all DOFs. Figure 8.17 display the relative distance between the tower and the blade tip with operational loads.

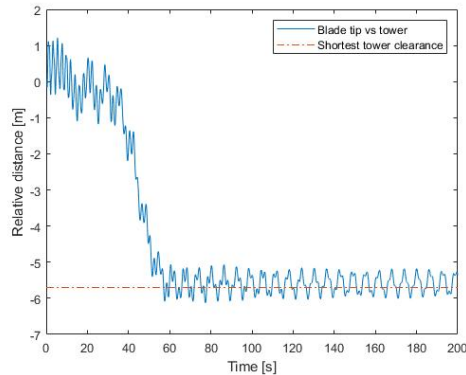


Figure 8.17: Relative distance between tower and blade tip

The relative distance stabilize around 5.7 m. The validity of this result is compared to blade deflection analyses performed for the 10 MW reference turbine. The rated wind speed of 11.4 m/s can cause the tip displacement to be around 10 m according to Sørum, Horn, and Amdahl (2017). Considering that the loads are multiplied by a factor of 0.5 in this thesis makes it reasonable to assume that the displacement given in Figure 8.17 is correct.

The operational loads cause the blades to utilize the full tower clearance in USFOS, and the result is valid when the tower top is fixed. In reality, the loads will cause the FOWT to move and tilt in the loading direction, and this will, in general, also affect the relative distance. However, this gives a good indication that the modeled clearance is too low.

Figure 8.19 display the relative distance in normal operation, and it is clear that the clearance is exceeded. One of the problems with this figure is to determine at what position the blade is located parallel to the turbine tower. Some of the measurements are close to 20 m in absolute value, and based on the structural behavior of the FOWT in operation, the maximum measurements in absolute value are considered to be when the turbine blade is at the top position. With reference to Figure 8.18 this is a reasonable assumption.

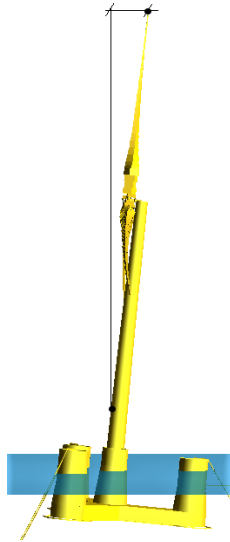


Figure 8.18: Structural behavior during normal operation

Additionally, the minimum measurements in absolute value are considered to be when the turbine blade is parallel to the tower. The relative distance is then approximately equal to the tower clearance, which coincides well with the deflection measured for the turbine blades.

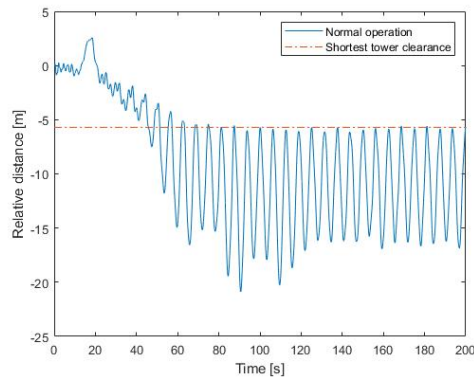


Figure 8.19: Relative distance between tower and blade tip in normal operation

Figure 8.20 display the relative distance when bulbous bow and side impact is initiated after 120 seconds. As seen, there is a significant disturbance in the results after the collision. This means that the relative displacement is worsened due to the collision. Some measurements are around -10 m in relative displacement after ship collision, and impact in USFOS is therefore reasonable to assume.

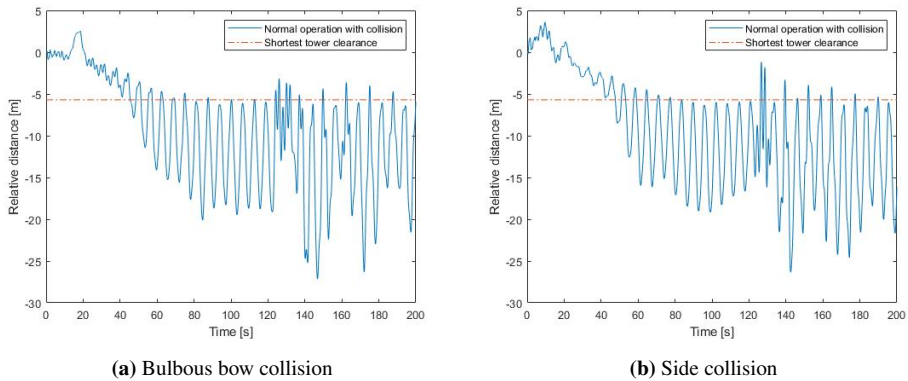


Figure 8.20: Relative distance between tower and blade tip with impact after 120 seconds.

The figures presented in this section display a risk for the turbine blades hitting the tower. The modeled clearance in USFOS is not sufficient, and during normal operation, the clearance is fully utilized. The relative displacement is worsened by 3-4 m due to a ship collision, so it is reasonable to assume that this action causes the blade to hit the tower. On the other hand, the real reference turbine has a clearance of 18.3 m. Using the same analogy as presented in this section makes it logical to assume that impact is unlikely to occur. It should also be mentioned that the operational loads are scaled by a factor of 0.5. Using the calculated forces as they are yield larger deflection and different results.

8.3.4 Mooringline forces

Collision scenarios considered with the spring system modeled in USFOS is based on considerations that the striking ship detach from the platform after the collision. However, a scenario where the two structures are locked together after impact is also possible. For this impact scenario, the interesting question is whether or not the mooring lines are capable of stopping the moving bodies. The procedure for evaluating this in USFOS starts by determining a force-displacement curve for the mooring line exposed to the largest forces. In operation, the FOWT takes some time until it is stable, and for the model in USFOS, stability is reached after around 100 seconds. For that matter, it is reasonable to add additional loading or other impacts after this point.

The force-displacement curve for the mooring line is created by adding a linearly increasing lateral force at the tower intersection. The force is applied in the same global direction as the incoming wind, and it is initiated after 100 seconds. For this scenario, only one mooring line is taking up the additional force, and this is the most severe case. The reference point for the force-displacement curve is taken after 100 seconds, and the result is displayed in Figure 8.21.

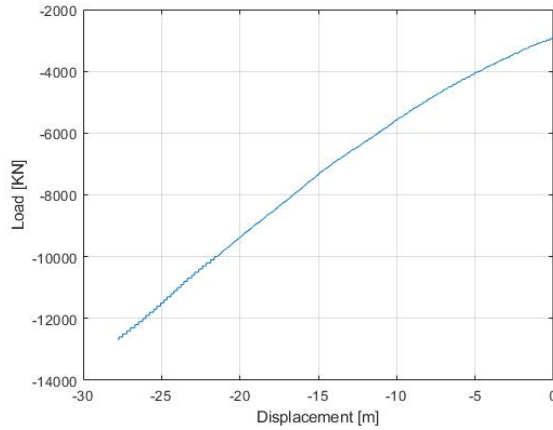


Figure 8.21: Force-displacement curve mooring line

The collision energies are 21 MJ and 37 MJ for ship side and bow, respectively. The amount of energy that is dissipated as strain energy can be calculated based on:

$$E_s = \frac{1}{2} (m_s + a_s) v_s^2 \frac{\left(1 - \frac{v_i}{v_s}\right)^2}{1 + \frac{m_s + a_s}{m_i + a_i}} \quad (8.12)$$

where the velocity of the installation is disregarded, i.e. $v_i=0$. Further, the added mass of the floating installation is considered to be of the same magnitude as for the ship. Hence, the equation is simplified to:

$$E_s = \frac{1}{2} (m_s + a_s) v_s^2 \frac{1}{1 + \frac{m_s}{m_i}} \quad (8.13)$$

Inserting properties give 16.7 MJ and 29.4 MJ dissipated as strain energy for side and bow collision, respectively. That means that for side collision 4.3 MJ remains kinetic, while for bow impact 7.6 MJ remains kinetic. The remaining kinetic energy is dissipated by work.

The work is calculated by integrating the force-displacement curve, and the areas under the curve should equal 4.3 MJ for side impact and 7.6 MJ for bow impact. The initial configuration for these calculations can be determined in two ways:

1. The instant effects from the ship collision can be disregarded. This means that the reference point is taken after 100 seconds.
2. The instant effects from the ship collision are included. This means that the displacement and mooring line force after impact is considered, which means that the reference point is shifted.

The latter method is used in this thesis as this yields the largest axial forces in the mooring line. Ship impact by side and bulb are initiated after 100 seconds, and the lateral displacements are 5.2 m and 4.8 m for bow and side, respectively. These two displacements are

therefore used as reference points, and the work is computed until it equals the remaining kinetic energy. The integration procedure is displayed in Figure 8.22.

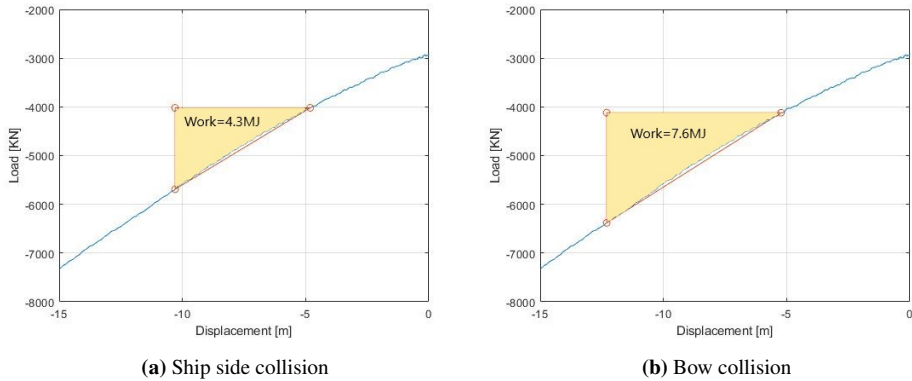


Figure 8.22: Force-displacement curve mooring line

The final axial loads that occur in the mooring line are 6.38 MN and 5.69 MN after impacts by bow and side, respectively. Code formulation for offshore mooring chains is used to determine if the strength is sufficient.

The breaking load of the mooring line can be determined based on the chain diameter. According to *Lifes50plus - Innovative floating offshore wind energy* (2020), the physical chain diameter is 137 mm. Offshore mooring chains are classified into five grades: R3, R3S, R4, R4S and R5. The breaking loads for the mooring chain are calculated according to *DNVGL-OS-E302* (2015). The result is summarized in Table 8.11.

Chain diameter [mm]	Breaking load [kN]				
	R3	R3S	R4	R4S	R5
137	13 829	15 441	16 992	18 852	19 844

Table 8.11: Breaking load for mooring chain

Another interesting measure is the proof load, which is the load that can be withstood without deformation.

Chain diameter [mm]	Proof load [kN]				
	R3	R3S	R4	R4S	R5
137	9673	11 162	13 395	14 883	15 565

Table 8.12: Proof load for mooring chain

The working load limit is the maximum load that should ever be applied to the product, and a rule of thumb is to apply a ratio of 3 to 1 on the braking load limit. That means that the working load limits can be expressed as:

Chain diameter [mm]	Working load limit [KN]				
	R3	R3S	R4	R4S	R5
137	4609	5147	5554	6284	6614

Table 8.13: Working load limit for mooring chain

The maximum mooring forces are compared to the working load limit for a 137 mm chain in Figure 8.23. The working load limit is below the maximum force in the line for most of the chain grades.

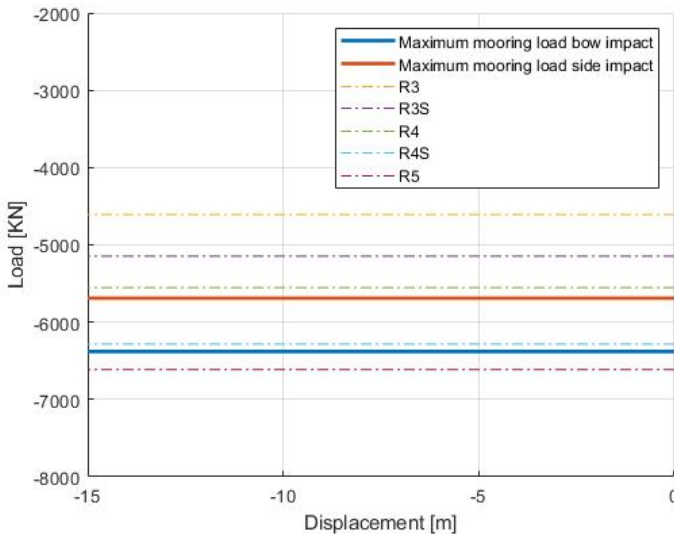


Figure 8.23: Maximum mooring line force compared to code specifications

The worst scenario is, as expected, bow collision. For this impact, a large portion of the collision energy remains kinetic, meaning that the mooring lines must dissipate a more significant amount of energy than for side impact.

An issue regarding the figure is that a ship collision is rare, and the accidental loads occurring from this impact might not be compared to the working load limit. Using the breaking load or proof load is a more reasonable criterion. For a 137 mm chain, the maximum loads from the collision are much lower than these limits. Hence, the mooring line can withstand the forces occurring for an impact scenario where the two bodies are locked to each other.

8.3.5 Operation in damaged condition

Accidental limit state correspond to survival conditions in a damaged condition (DNVGL-ST-0119 2018). Designing a structure against accidental loads serves the purpose that the structural integrity is not impaired by, for instance, a collision. In Chapter 7, punching shear failure is investigated, and for a concrete wall thickness of 0.4 m, this failure phenomena is possible. Flooding of compartments is a result if this happens, and the structural post-damage resistance needs to be evaluated.

The floating structure is often divided into compartments to provide sufficient integrity, and compartmentalization of OO-Star Wind Floater is reasonable to assume. However, this information is not public, so the volume that can be flooded after a collision is difficult to determine.

For ship collision by bow, the bulb center is 1.5 m below MSL, and penetration of the column wall at this location is assumed. Further, the flooded compartment is assumed to be 2.4 m in height, extending from MSL to 2.4 m below MSL. This gives a volume of 343 m³ that is filled with seawater. At this flooding level, the structural integrity is sufficient to withstand the loads from normal operation of the turbine. The FOWT is, therefore, safe until maintenance work can be performed. Additional evaluation is performed by flooding a larger volume. The new volume extends from MSL to 4 m below MSL, giving a flooded volume of 564 m³. For this flooding configuration, the structure capsizes. This is a catastrophic scenario in terms of environmental and economic impact.

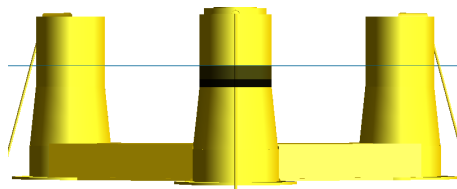


Figure 8.24: Flooded compartments

Basic hand calculations can be utilized to determine the damage stability. Initially, the metacentric height needs to be calculated:

$$GM = KB + BM - KG \quad (8.14)$$

where KB and KG are extracted from the USFOS model, with values of 6.6 m and 10.6 m, respectively. BM is calculated by the 2nd moment of the waterplane area and the displacement.

$$BM = \frac{I}{\nabla} \quad (8.15)$$

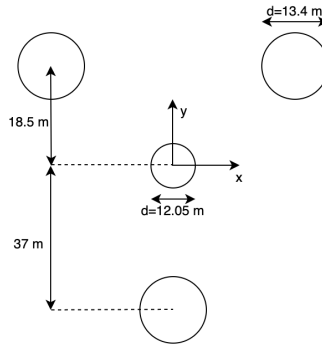


Figure 8.25: Waterplane OO-Star Wind Floater

Inserting into Equation 8.14 result in a metacentric height of 8.6 m.

Capsizing of the structure is considered to be when the outer column submerges, and by using the geometry properties in Figure 8.25, this occur for an heeling angle of 13.4° , or 9.5 m submergence. In operational condition, the general loading of the structure cause an heeling angle of 3.5° . Additional overturning moment by flooding around 560 m^3 cause the structure to capsize in USFOS. This can be verified by simple hand calculations. The overturning moment from this flooding volume can be calculated as:

$$M_o = V_{flooded} * \rho_{seawater} * g * arm = 560 * 1025 * 9.81 * 37 = 2.08E + 08Nm \quad (8.16)$$

The uprighting moment is calculated by:

$$M_u = Weight * GM * \sin(\phi) \quad (8.17)$$

Equilibrium is reached for a heeling angle of 5° . The total heeling of the structure is therefore 8.5° , giving a submergence of 6 m. In addition, the extra weight cause the floating structure to submerge one meter. That gives a total submergence of 7 meter, while the clearance is around 9.5 m. Based on these calculations, the structure will not capsize. However, in USFOS it does. One of the reason for this can be that the draft is somewhat different in USFOS than for the real model. Another reason can be disturbance from the operational loads, inducing extra overturning moment. On the other hand, the result is based on simplifications, and small differences is reasonable.

The exact volume that can be flooded for the real structure is challenging to determine, but based on the scenarios considered here, there have to be watertight compartments in the columns. Structural drawings for the floater will increase the accuracy of these calculations.

Discussion and conclusion

Floating offshore installations are necessary to utilize the full potential from offshore wind, and like all other offshore installations, they are subjected to the risk of ship collisions. Various code formulations exist for designing floating wind turbine structures against accidental actions, and in this thesis, the most relevant have been presented.

Future floating wind farms can be located close to ship traffic lanes. Additionally, moving them farther offshore introduces more hostile environments and larger service vessels. These effects increase the risk of ship collisions, and accidents between service vessels and FOWT is a general concern. The consequences can range from small to major, i.e., from repair cost to injuries and fatalities. Proper investigations of this accidental action are therefore necessary.

Nonlinear analyses in LS-DYNA and USFOS have been performed for OO-Star Wind Floater. The FOWT substructure is built in concrete, making strength design the most proper design principle. For concrete structures subjected to concentrated loads, punching shear is a failure mechanism that can have severe consequences. This phenomenon has been investigated in LS-DYNA, and comparison to concrete rule formulations have been performed. The thickness of the concrete wall is an important parameter, and this information is not publicly available for OO-Star Wind Floater. For that matter, parameter study on different column thicknesses has been conducted. Punching shear failure occurs when the thickness is 0.4 m or less, and flooding of watertight compartments is the result. This impairs the general stability of the structure significantly, so this is a failure mechanism that is important to consider in the design. More thorough analyses should be based on actual properties for the concrete, i.e., column thickness, concrete specifications and reinforcement ratio. Structural drawings, including the watertight compartments, are also necessary to evaluate the risk more accurately.

Global response analyses have been performed in USFOS, where various collision scenarios have been investigated. The FOWT can be in either parked or operational condition,

so both these states have been studied. The turbine tower is an unstiffened cylindrical shell, and local buckling is a risk during a ship impact. In general, this phenomena is most critical for impacts occurring normal to the rotor plane. There is no risk for elastoplastic buckling in parked condition, but in operational condition, some of the utilization factors are close to the limit. For that matter, a shell element substructure has been created at the lower part of the tower. Buckling does not occur for velocities according to rule formulations, but by increasing the impact velocity for broadside collision to 5 m/s, local buckling occurs. The buckling causes the tower to fall in the direction of the ship. Adjustments to the design are recommended to prevent this from happening.

Accelerations of the nacelle pose a threat to the electrical equipment, and exceeding 0.2-0.3g can have severe economic consequences. The results from both parked and operating turbine states that this limit is exceeded for many of the collision scenarios.

The tower clearance is a measure of the lowest distance between the blade tip and the tower. The 10 MW RWT has a clearance of 18.3 m, while the model in USFOS has a clearance of 5.7 m. The consequences of the blade hitting the tower include maintenance work, loss of electricity production and pollution. During collision in both parked and operational condition, this risk is present in USFOS. However, taking the clearance for the reference turbine into consideration, this event is unlikely to occur. It should be mentioned that the operational loads have been reduced in this thesis by a factor of 0.5. The deflection of the blades utilizes the full clearance with this loading, which indicates that the modeled clearance is insufficient. If the original loads are going to be used, it is recommended that the tower clearance is modeled more accurately.

Punching shear failure influence the structural integrity of the FOWT. The structure cap-sizes for a flooded volume of 564 m³. According to codes, the structure is inadequate if the watertight compartment around the impact location is of this size. An issue regarding these calculations is that the heeling angle for the structure during normal operation is overestimated in USFOS. The ballast system will stabilize the real structure, so the FOWT is assumed to be able to withstand a larger flooding volume.

Collision scenarios where the two bodies are locked to each other are also investigated. For this impact, the interesting question is whether or not the mooring lines are capable of stopping the moving bodies. Considering the worst scenario possible it is reasonable to assume that the lines have sufficient strength.

A general conclusion is that accidental loads from a ship collision are critical for the FOWT. Economic losses are probable consequences, but health and safety are also impaired. Accurate investigations are therefore recommended.

Chapter 10

Further work

Ship collision on parked and operating turbine have been considered. No forces from the wind have been accounted for in parked condition, and this is a questionable assumption. Generally, wind forces are always present, and in the event of for instance maintenance work, the loads can be significant. Including wind loads also in parked condition is proposed.

Environmental loading on the structure occur from waves and wind, and the modeled wave is a Stoke wave with insignificant height. Investigating the response in worse sea states is interesting. For all the analyses, rotation of the rotor plane is also proposed. This will influence the stability and response during the different ship impacts.

Obtaining more accurate description of OO-Star Wind Floater is recommended. This includes:

- Thickness of the concrete columns.
- Reinforcement ratio.
- Concrete properties.
- Structural drawings with information regarding watertight compartments.
- Characteristics of the active ballast system.

These properties will yield more accurate results, for instance for the punching shear analyses. In this thesis these calculations are based on multiple assumptions.

The turbine model is based on the 10 MW reference wind turbine. One of the characteristics that has been simplified is the tower clearance. Modeling this more accurately, i.e., including precone and tilt is recommended. The full operational loads may then be applied, giving more accurate and realistic results. This is especially valuable in the investigations

of the relative distance between the turbine and the blades. Additionally, modeling one of the turbine blades parallel to the tower is recommended in parked condition. Regarding operational condition, the displacement of the turbine blades are large. Local buckling of the blades can be investigated.

The length of the mooring lines has been reduced in this thesis, and axial loads at the sea bottom has been used to obtain the correct shape and pretension. More accurate modelling of these lines are recommended, i.e., to include the full length and still obtain the correct properties.

Finally, the number of collision scenarios can be increased. That means including different ship types and different velocities.

Bibliography

- Amdahl, Jørgen (Nov. 2010). “Chapter 5: Buckling of Cylindrical Shells”. TMR4205 Buckling and Ultimate Strength of Marine Structures. MTS.
- (Feb. 2013). “Chapter 2: Buckling of Bars and Frames”. TMR4205 Buckling and Ultimate Strength of Marine Structures. MTS.
- Amdahl, Jørgen and Tore Holmås (2011). “High energy ship collisions with jacket supported offshore wind turbines”. Proceedings of the international conference on computational methods in marine engineering. Barcelona, Spain.
- Amdahl, Jørgen, Gunnar Solland, and Arnfinn Reitan (Oct. 2017). DNVGL-RP-C204 Design against accidental loads. DNV GL AS.
- Bak, Christian et al. (July 2013). Description of the DTU 10 MW Reference Wind Turbine. DTU Wind Energy.
- Bela, Andreea et al. (Jan. 2017). Ship collision analysis on offshore wind turbine monopile foundations. en. *Marine Structures* 51, pp. 220–241. ISSN: 0951-8339. DOI: 10 . 1016/j.marstruc.2016.10.009. URL: <http://www.sciencedirect.com/science/article/pii/S0951833916302519> (visited on 05/08/2020).
- Biehl, Florian and Eike Lehmann (2006). “Collisions of Ships with Offshore Wind Turbines: Calculation and Risk Evaluation”. en. *Offshore Wind Energy*. Ed. by Julia Köller, Johann Köppel, and Wolfgang Peters. Springer Berlin Heidelberg, pp. 281–304. ISBN: 978-3-540-34676-0. DOI: 10 . 1007/978-3-540-34677-7_17. URL: http://link.springer.com/10.1007/978-3-540-34677-7_17 (visited on 05/11/2020).
- Brøndsted, Povl and Rogier P.L Nijssen (2013). *Advances in wind turbine blade design and materials*. Woodhead Publishing series in energy 47. Philadelphia, PA: Woodhead Pub.
- Christensen, C F, L W Andersen, and P H Pedersen (2001). *Ship Collision Risk for an Offshore Wind Farm*. en, p. 7.
- Cox, Kevin and Andreas Echtermeyer (Jan. 2012). Structural Design and Analysis of a 10MW Wind Turbine Blade. en. *Energy Procedia*. Selected papers from Deep Sea Offshore Wind R&D Conference, Trondheim, Norway, 19-20 January 2012 24, pp. 194–201. ISSN: 1876-6102. DOI: 10 . 1016/j.egypro.2012.06.101. (Visited on 01/29/2020).

-
- Dai, Lijuan et al. (Jan. 2013). Risk of collision between service vessels and offshore wind turbines. en. *Reliability Engineering & System Safety* 109, pp. 18–31. ISSN: 0951-8320. DOI: 10.1016/j.ress.2012.07.008. URL: <http://www.sciencedirect.com/science/article/pii/S0951832012001585> (visited on 05/08/2020).
- DNV-RP-C202 (2013). DNV-RP-C202: Buckling Strength of Shells. en. Høvik, Norway: DNV GL.
- DNVGL-OS-C401 (July 2015). DNVGL-OS-C401-Fabrication and testing of offshore structures. DNV GL Høvik, Norway. URL: <https://rules.dnvgl.com/docs/pdf/dnvgl/OS/2015-07/DNVGL-OS-C401.pdf>.
- DNVGL-OS-E302 (July 2015). DNVGL-OS-E302-Offshore mooring chain. Høvik, Norway: DNV GL. URL: <https://rules.dnvgl.com/docs/pdf/dnvgl/OS/2015-07/DNVGL-OS-E302.pdf>.
- DNVGL-ST-0119 (July 2018). Floating wind turbine structures.
- Echeverry, Sara et al. (2019). Numerical Crashworthiness Analysis of a Spar Floating Offshore Wind Turbine Impacted by a Ship. *Developments in the collision and grounding of ships and offshore structures*.
- Eurocode 2 (Dec. 2004). Eurocode 2: Design of concrete structures - Part 1-1 : General rules and rules for buildings. British Standard Institution.
- Frøyd, Lars and Ole G Dahlhaug (n.d.). Rotor Design for a 10 MW Offshore Wind Turbine. en (), p. 8.
- Goerlandt, Floris and Pentti Kujala (Jan. 2011). Traffic simulation based ship collision probability modeling. en. *Reliability Engineering & System Safety*. Special Issue on Safecomp 2008 96.1, pp. 91–107. ISSN: 0951-8320. DOI: 10.1016/j.ress.2010.09.003. URL: <http://www.sciencedirect.com/science/article/pii/S0951832010002061> (visited on 01/21/2020).
- Hong, Lin (2009). “Simplified analysis and design of ships subjected to collision and grounding”. PhD thesis. Norges teknisk-naturvitenskapelige universitet, Fakultet for ingeniørvitenskap og teknologi, Institutt for marin teknikk.
- Hong, Lin, Jørgen Amdahl, and Ge Wang (June 2009). A Direct Design Procedure for FPSO Side Structures Against Large Impact Loads. *Journal of Offshore Mechanics and Arctic Engineering* 131.031105. ISSN: 0892-7219. DOI: 10.1115/1.3124140. URL: <https://doi.org/10.1115/1.3124140> (visited on 05/26/2020).
- Kitamura, O. (July 2002). FEM approach to the simulation of collision and grounding damage. en. *Marine Structures. Ship Collisions and Grounding* 15.4, pp. 403–428. ISSN: 0951-8339. URL: <http://www.sciencedirect.com/science/article/pii/S0951833902000102> (visited on 05/26/2020).
- Kvitrud, Arne (Jan. 2011). Collisions Between Platforms and Ships in Norway in the Period 2001-2010. en. Volume 2: Structures, Safety and Reliability. Rotterdam, The Netherlands: ASMEDC, pp. 637–641. ISBN: 978-0-7918-4434-2. DOI: 10.1115/OMAE2011-49897. URL: <https://asmedigitalcollection.asme.org/OMAE/proceedings/OMAE2011/44342/637/341443> (visited on 05/11/2020).
- Lifes50plus - Innovative floating offshore wind energy (2020). en-US. URL: <https://lifes50plus.eu/> (visited on 02/04/2020).
-

-
- LS-DYNA Theory Manual (July 2019). URL: http://ftp.lstc.com/anonymous/outgoing/jday/manuals/DRAFT_Theory.pdf (visited on 02/19/2020).
- Moan, Torgeir (Sept. 2003). “Nonlinear analysis”. Finite element modelling and analysis of marine structures. Department of Marine Technology.
- Moulas, D., M. Shafiee, and A. Mehmanparast (Oct. 2017). Damage analysis of ship collisions with offshore wind turbine foundations. en. *Ocean Engineering* 143, pp. 149–162. ISSN: 0029-8018. URL: <http://www.sciencedirect.com/science/article/pii/S0029801817302445> (visited on 05/11/2020).
- N-003, NORSOK (2017). Actions and action effects. 3rd ed. NORSOK STANDARD.
- N-004, NORSOK (2004). Design of steel structures. 2nd ed. NORSOK STANDARD.
- Key trends and statistics 2019 (Feb. 2020). Offshore Wind in Europe-Key trends and statistics 2019. URL: <https://windeurope.org/wp-content/uploads/files/about-wind/statistics/WindEurope-Annual-Offshore-Statistics-2019.pdf> (visited on 05/13/2020).
- Olav Olsen AS, Dr. techn. (2020). Breakthrough for OO-Star Wind Floater. Library Catalog: www.olavolsen.no. URL: <https://www.olavolsen.no/no/aktuelt/post-hdQPQ-breakthrough-for-oo-star-wind-floater> (visited on 05/22/2020).
- Presencia, Carla E. and Mahmood Shafiee (July 2018). Risk analysis of maintenance ship collisions with offshore wind turbines. *International Journal of Sustainable Energy* 37.6, pp. 576–596. ISSN: 1478-6451. DOI: 10.1080/14786451.2017.1327437. URL: <https://doi.org/10.1080/14786451.2017.1327437> (visited on 05/08/2020).
- Bureau of Ocean Energy Management (2020). Renewable Energy on the Outer Continental Shelf — Bureau of Ocean Energy Management. URL: <https://www.boem.gov/renewable-energy/renewable-energy-program-overview> (visited on 05/22/2020).
- Sha, Yanyan and Jørgen Amdahl (Jan. 2019). Numerical investigations of a prestressed pontoon wall subjected to ship collision loads. en. *Ocean Engineering* 172, pp. 234–244. ISSN: 0029-8018. URL: <http://www.sciencedirect.com/science/article/pii/S0029801818315476> (visited on 05/05/2020).
- Sørum, Stian Høegh, Jan-Tore H. Horn, and Jørgen Amdahl (Oct. 2017). Comparison of numerical response predictions for a bottom-fixed offshore wind turbine. en. *Energy Procedia*. 14th Deep Sea Offshore Wind R&D Conference, EERA DeepWind’2017 137, pp. 89–99. ISSN: 1876-6102. DOI: 10.1016/j.egypro.2017.10.336. URL: <http://www.sciencedirect.com/science/article/pii/S1876610217352979> (visited on 05/28/2020).
- Storheim, Martin (Aug. 2015). “Structural response in ship-platform and ship-ice collisions”. PhD thesis. Norges teknisk-naturvitenskapelige universitet, Fakultet for ingeniørvitenskap og teknologi, Institutt for marin teknikk.
- Caithness Windfarm Information Forum (2020). Summary of Wind Turbine Accident data to 31 March 2020. URL: <http://www.caithnesswindfarms.co.uk/AccidentStatistics.htm> (visited on 05/11/2020).
- USFOS - Reality Engineering (2020). URL: <https://www.usfos.no/> (visited on 02/05/2020).
-

-
- USFOS Gettin Started (June 2001).
- USFOS USER'S MANUAL-MODELLING (Feb. 1999). URL: https://www.usfos.no/manuals/usfos/users/documents/Usfos_UM_03.pdf.
- Veritas-NI-572, Bureau (Jan. 2019). Classification and Certification of Floating Offshore Wind Turbines. Bureau Veritas.
- Wang, Ge, Kikuo Arita, and Donald Liu (May 2000). Behavior of a double hull in a variety of stranding or collision scenarios. en. *Marine Structures* 13.3, pp. 147–187. ISSN: 0951-8339. DOI: 10.1016/S0951-8339(00)00036-8. URL: <http://www.sciencedirect.com/science/article/pii/S0951833900000368> (visited on 05/26/2020).
- Wang, Xuefei et al. (Feb. 2018). A review on recent advancements of substructures for offshore wind turbines. en. *Energy Conversion and Management* 158, pp. 103–119. ISSN: 0196-8904. DOI: 10.1016/j.enconman.2017.12.061. URL: <http://www.sciencedirect.com/science/article/pii/S019689041731213X> (visited on 05/22/2020).
- Wind energy today (2020). Library Catalog: [windeurope.org](http://windeurope.org/about-wind/wind-energy-today/). URL: <https://windeurope.org/about-wind/wind-energy-today/> (visited on 05/22/2020).
- Yno 227 - Mærsk Frontier (2020). en. Library Catalog: [ulstein.com](http://ulstein.com/historic-references/yno-227-m%C3%A6rsk-frontier). URL: <https://ulstein.com/historic-references/yno-227-m%C3%A6rsk-frontier> (visited on 05/05/2020).
- Yu, Wei, Kolja Müller, and Frank Lemmer (Apr. 2018). D4.2 Public Definition of the Two LIFES50+ 10MW Floater Concepts. en, p. 32.
- Yu, Zhaolong et al. (Sept. 2016). Implementation of Linear Potential-Flow Theory in the 6DOF Coupled Simulation of Ship Collision and Grounding Accidents. en. *Journal of Ship Research* 60.3, pp. 119–144. ISSN: 00224502, 15420604. DOI: 10.5957/JOSR.60.3.160012. URL: <http://www.ingentaselect.com/rpsv/cgi-bin/cgi?ini=xref&body=linker&reqdoi=10.5957/JOSR.60.3.160012> (visited on 03/10/2020).
- Zineddin, M. and T. Krauthammer (Sept. 2007). Dynamic response and behavior of reinforced concrete slabs under impact loading. en. *International Journal of Impact Engineering. Design and Analysis of Protective Structures Against Impact/Impulsive/Shock Loads (DAPSIL)* 34.9, pp. 1517–1534. ISSN: 0734-743X. URL: <http://www.sciencedirect.com/science/article/pii/S0734743X06002740> (visited on 05/26/2020).

Punching shear check for concrete column

Punching shear checks for the concrete column are performed for both ship side and ship bow. For each of these impacts, one $1*1\text{ m}^2$ and $3*2\text{ m}^2$ area is used for extracting the shear force from LS-DYNA. The thickness of the concrete column is not known in advance, so three different thicknesses are considered, i.e 0.3, 0.4 and 0.5 m.

A.1 Ship side 1 m^2

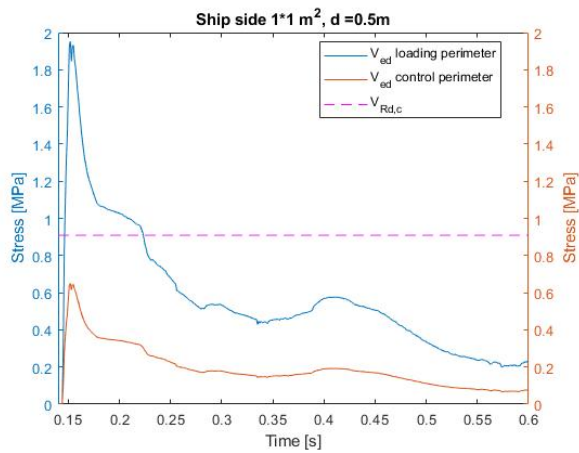


Figure A.1: Punching shear ship side, $d=0.5$

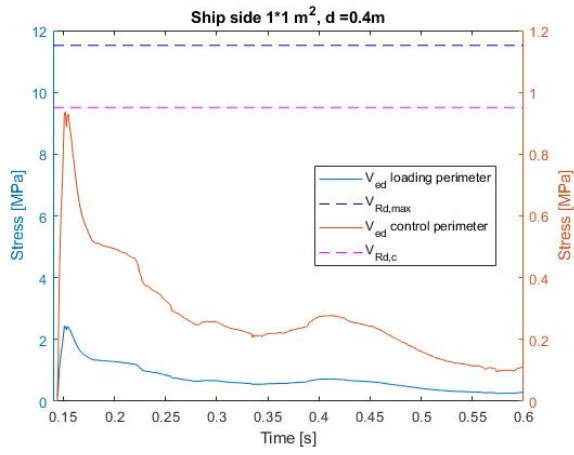


Figure A.2: Punching shear ship side, d=0.4

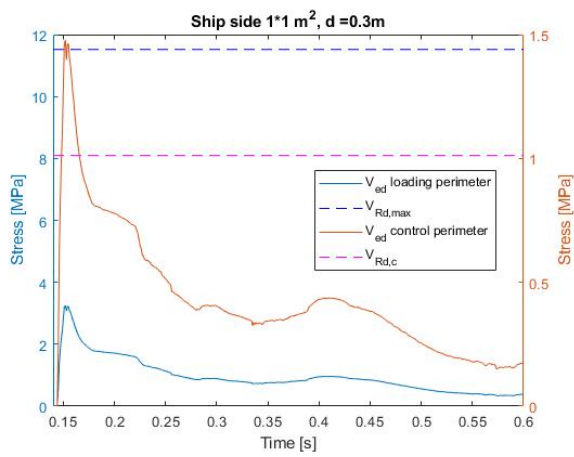


Figure A.3: Punching shear ship side, d=0.3

A.2 Ship side 6 m²

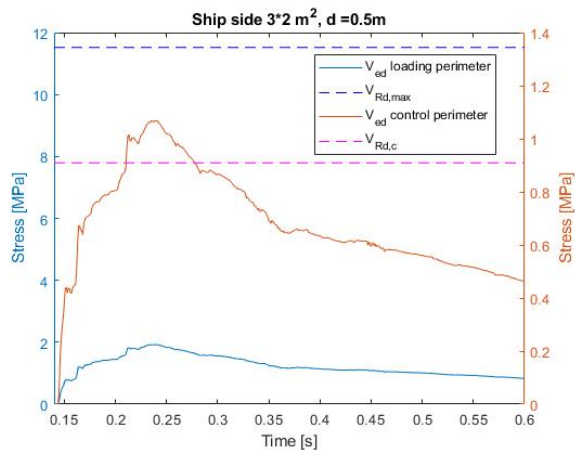


Figure A.4: Punching shear ship side, d=0.5

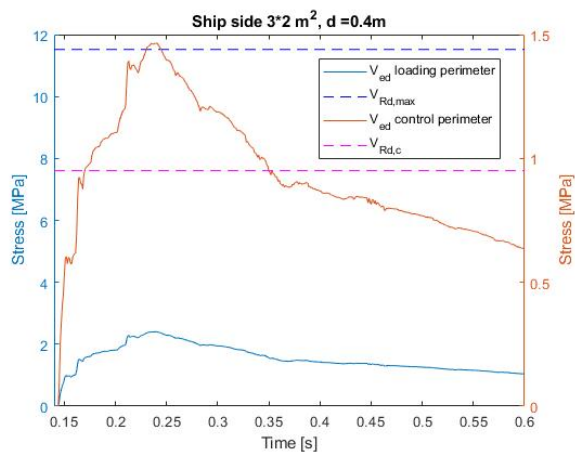


Figure A.5: Punching shear ship side, d=0.4

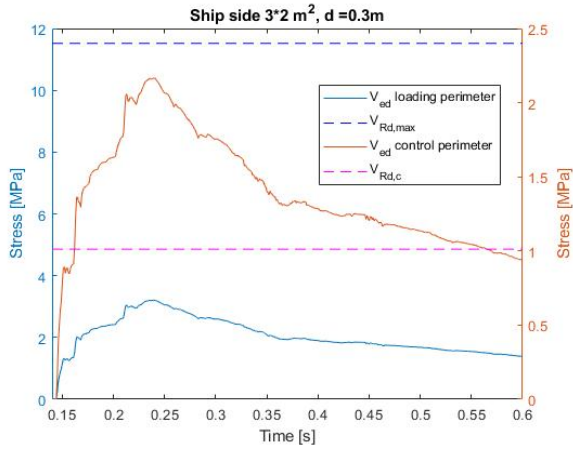


Figure A.6: Punching shear ship side, d=0.3

A.3 Ship bulb 1 m²

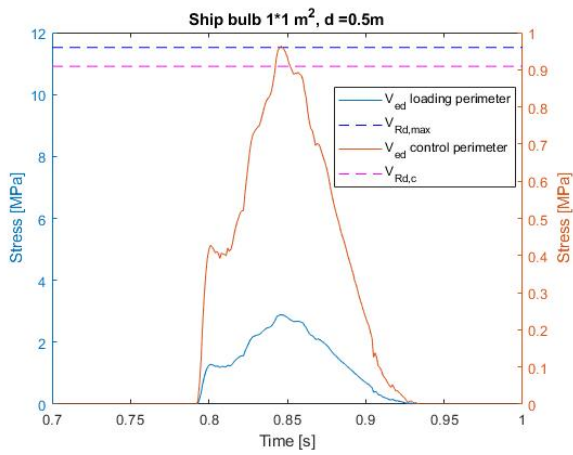


Figure A.7: Punching shear ship bulb, d=0.5

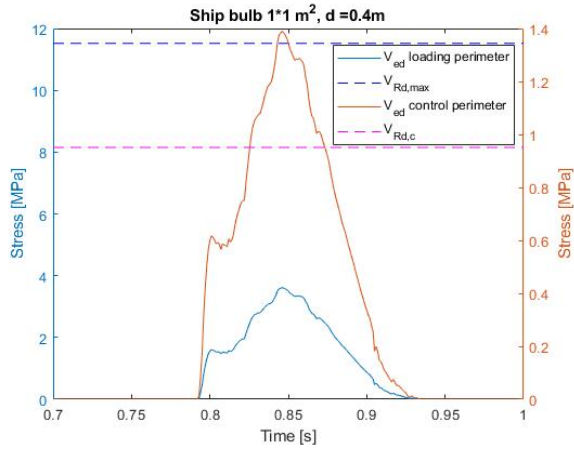


Figure A.8: Punching shear ship bulb, d=0.4

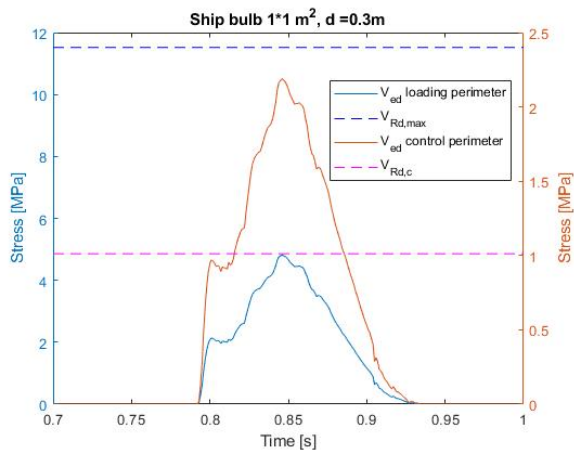


Figure A.9: Punching shear ship bulb, d=0.3

A.4 Ship bulb 6 m²

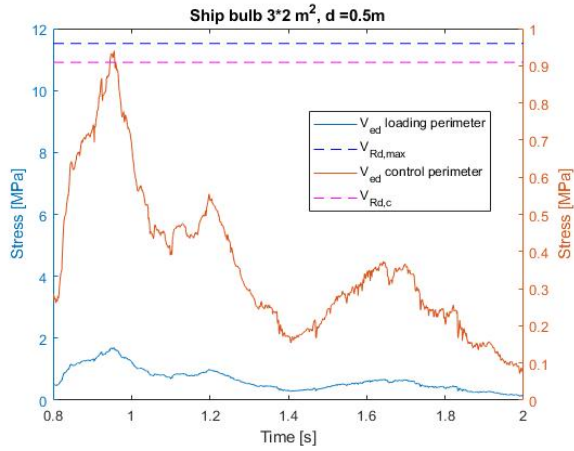


Figure A.10: Punching shear ship bulb, d=0.5

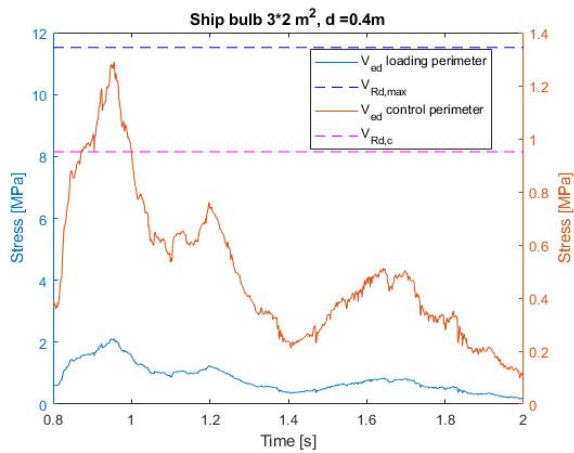


Figure A.11: Punching shear ship bulb, d=0.4

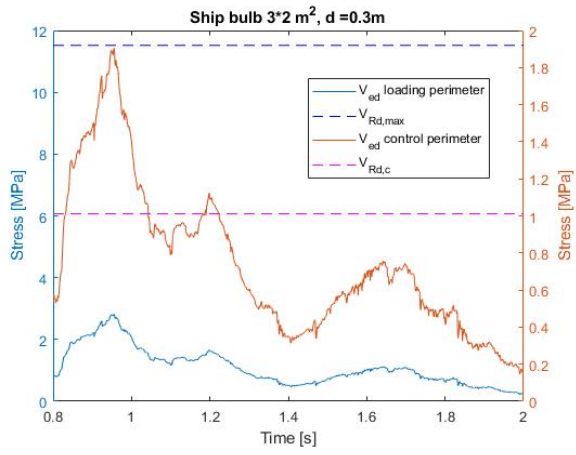


Figure A.12: Punching shear ship bulb, $d=0.3$

